Structure, infrared and Raman spectroscopic studies of newly synthetic AII(SbV0.50FeIII0.50)(PO4)2 (A = Ba, Sr, Pb) phosphates with yavapaiite structure

Abderrahim Aatiq, My Rachid Tigha, Rachid Fakhreddine, Damien Bregiroux, Gilles Wallez

Accepted Manuscript

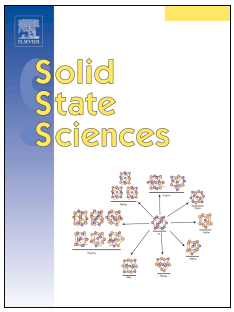

Structure, infrared and Raman spectroscopic studies of newly synthetic $A^{II}(Sb^{V}_{0.50}Fe^{III}_{0.50})(PO_4)_2$ (A = Ba, Sr, Pb) phosphates with yavapaiite structure

Abderrahim Aatiq, My Rachid Tigha, Rachid Fakhreddine, Damien Bregiroux, Gilles Wallez

PII: S1293-2558(16)30310-7

DOI: 10.1016/j.solidstatesciences.2016.05.009

Reference: SSSCIE 5326

To appear in: *Solid State Sciences*

Received Date: 2 November 2015

Revised Date: 25 February 2016

Accepted Date: 27 May 2016

Please cite this article as: A. Aatiq, M.R. Tigha, R. Fakhreddine, D. Bregiroux, G. Wallez, Structure, infrared and Raman spectroscopic studies of newly synthetic $A^{II}(Sb^{V}_{0.50}Fe^{III}_{0.50})(PO_4)_2$ (A = Ba, Sr, Pb) phosphates with yavapaiite structure, *Solid State Sciences* (2016), doi: 10.1016/j.solidstatesciences.2016.05.009.

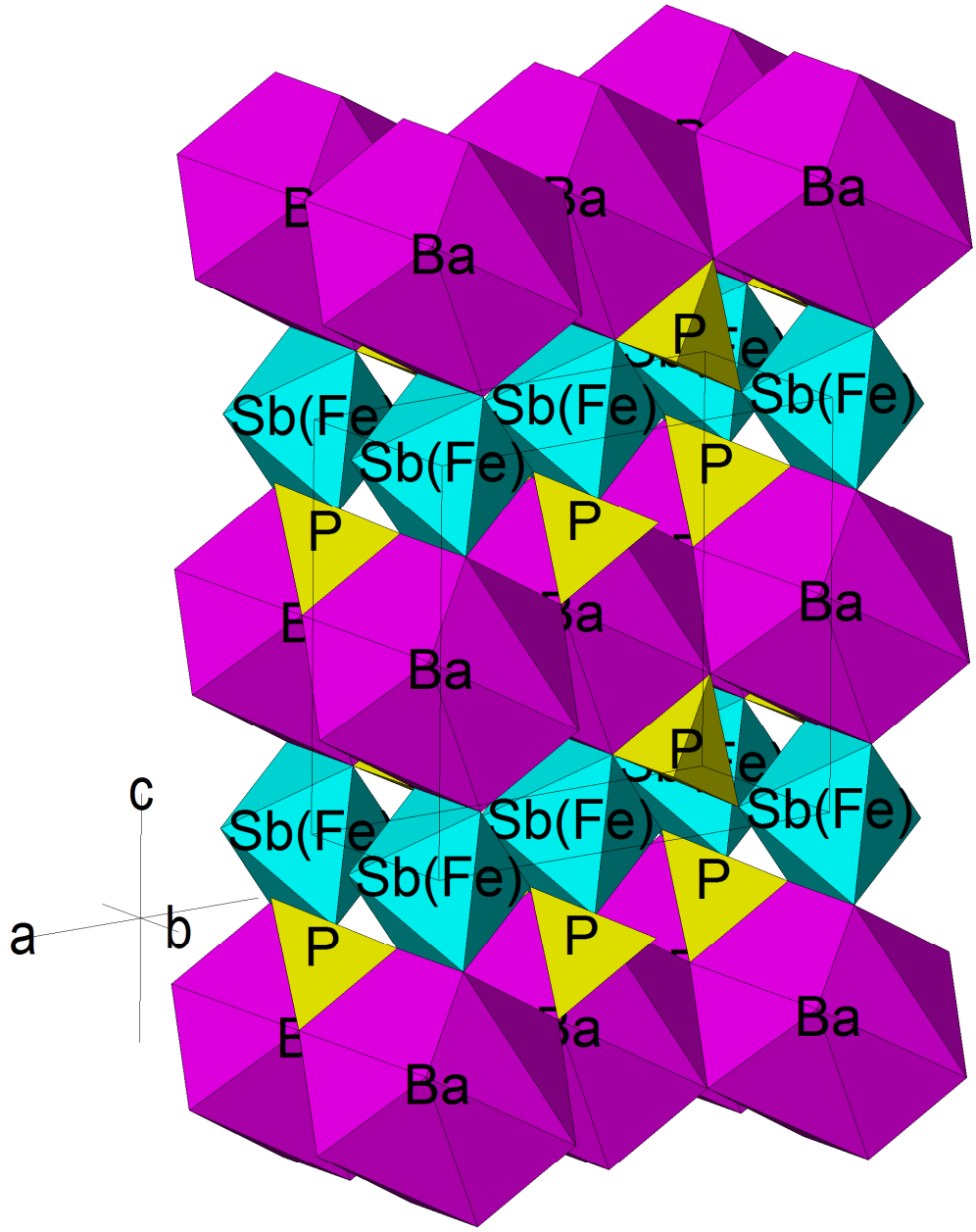
Ba
Sb(Fe)
P
c
a
b

Structure, Infrared and Raman spectroscopic studies of newly synthetic $A^{II}(Sb^{V}_{0.50}Fe^{III}_{0.50})(PO_4)_2$ (A = Ba, Sr, Pb) phosphates with yavapaiite structure

Abderrahim Aatiq[1], My Rachid Tigha[1], Rachid Fakhreddine[1], Damien Bregiroux[2] and Gilles Wallez[3,4]

[1] Université HassanII de Casablanca, Faculté des Sciences Ben M'Sik, Département de Chimie, Laboratoire de Physico-Chimie des Matériaux Appliqués, Avenue Idriss El harti, B.P. 7955, Casablanca, Morocco

[2] Sorbonne Universités, UPMC Univ Paris 06, CNRS, Collège de France, Laboratoire de Chimie de la Matière Condensée de Paris, 11 place Marcelin Berthelot, 75005 Paris, France

[3] Institut de Recherche de Chimie Paris (IRCP),CNRS – Chimie Paris Tech – Paris Sciences et Lettres PSL UMR8247,11 rue Pierre et Marie Curie,75005Paris, France

[4] Sorbonne Universités, UPMC Univ Paris 06, France

Abstract

The synthesis and structural study of three new $A^{II}(Sb^{V}_{0.5}Fe^{III}_{0.5})(PO_4)_2$ (A = Ba, Sr, Pb,) phosphates belonging to the A-Sb-Fe-P-O system were reported here for the first time. Structures of [Ba], [Sr] and [Pb] compounds, obtained by solid state reaction in air atmosphere, were determined at room temperature from X-ray powder diffraction using the Rietveld method. $Ba^{II}(Sb^{V}_{0.5}Fe^{III}_{0.5})(PO_4)_2$ [Ba] features the yavapaiite-type structure, with space group *C*2/*m*, Z = 2 and a = 8.1568(4) Å; b= 5.1996(3) Å c= 7.8290(4) Å; β = 94.53(1)°. $A^{II}(Sb^{V}_{0.5}Fe^{III}_{0.5})(PO_4)_2$ (A = Sr, Pb) compounds have a distorted yavapaiite structure with space group *C*2/*c*, Z = 4 and a = 16.5215(2) Å; b = 5.1891(1) Å c = 8.0489(1) Å; β = 115.70(1)° for [Sr]; a = 16.6925(2) Å; b = 5.1832(1) Å c = 8.1215(1) Å; β = 115.03(1)° for [Pb]. Raman and Infrared spectroscopic study was used to obtain further structural information about the nature of bonding in selected compositions.

Keywords: Antimony and Iron phosphate; yavapaiite structure; Raman and IR spectroscopy; Rietveld analysis.

Abbreviations: $Ba^{II}(Sb^{V}_{0.5}Fe^{III}_{0.5})(PO_4)_2$ = [Ba], $Sr^{II}(Sb^{V}_{0.5}Fe^{III}_{0.5})(PO_4)_2$ = [Sr], $Pb^{II}(Sb^{V}_{0.5}Fe^{III}_{0.5})(PO_4)_2$ = [Pb], *TY* = True Yavapaiite, *DY* = Distorted Yavapaiite.

Introduction

Crystal structures of $A_{(1-x)}A'_xPO_4$ phases have been revealed in previous studies. Such materials can include a mixing of A^{II}/A'^{IV} ions leading to $(A^{II}_{0.5}A'^{IV}_{0.5})PO_4$ phases [1-3] or a mixture of A^{II}, A'^{III} and A''^{IV} ions as in the case of $A^{II}_{1/3}A'^{III}_{1/3}A''^{IV}_{1/3}PO_4$ (A^{II} = Mg, Ca, Cd, Sr; A'^{III} = Sm, Gd, Nd ; A''^{IV} = Zr, Ce, Th) compounds [4]. As a result of various cationic substitution in A sites of $A^{III}PO_4$ phases, new family of oxides crystallizing in several structural types as Monazite, Zircon (Xenotime), Scheelite, Cheralite, Nasicon and Yavapaiite type compounds have been synthesized and characterized [1-18]. For smaller M^{IV} ions, as in the $Ba^{II}_{0.5}M^{IV}_{0.5}PO_4$ (M^{IV} = Ti, Zr, Hf, Ge, Sn, Mo) series, a monoclinic structure isotypic of the $K_{0.5}Fe_{0.5}SO_4$ yavapaïte (*C*2/*m* space group) is obtained [6-9]. Note that these phases have a structure which is made of layers of Ba^{II} cations in tenfold coordination, alternating with dense slabs built up of corner-connected of $M^{IV}O_6$ octahedra and PO_4 tetrahedra. This structure changes into a trigonal one at high temperature (*P*-3*m*1) through a simple mechanism involving the unfolding of the $[M(PO_4)_2]_n^{2-}$ layers [19]. Numerous compounds among the $A^{II}M^{IV}(PO_4)_2$ (A= Ba, Pb, Sr, Ca; M = Ge, Ti, Mo, Zr, Sn, Pu, Np, U, Th) family have structures which are related to the yavapaiite type structure. In fact, their structure is strongly dependant to the nature and/or size of the A^{II} and M^{IV} cations. More recently the relationships between composition and crystal structure of some $A^{II}M^{IV}(PO_4)_2$ compounds are established [20]. Thus, Morin et al. have shown that the structure of $PbSn(PO_4)_2$ (space group $P2_1/n$**)** is related to the yavapaiite type but the lead atoms are located in zigzag tunnels instead of layers [10]. This last structure was explained by the presence of an active Pb^{II} lone pair which has been localized from electrostatic interactions. The $AZr(PO_4)_2$ (*A*=Ca, Sr and Ba) have a different crystal structure at room temperature. Whereas $BaZr(PO_4)_2$ has a monoclinic yavapaiite structure, the $SrZr(PO_4)_2$ is triclinic ($P\bar{1}$ space group) at room temperature and during heating, the compound shows two other polymorphic forms. $SrZr(PO_4)_2$ undergoes a triclinic to monoclinic transition at 405 K, and then to trigonal at 1196K [11]. Structural study of the $SrZr(PO_4)_2$–$BaZr(PO_4)_2$ system reveals the occurrence of two phase transitions during heating and the space group has changed from *P*2/*c* to *C*2/*m* at 400 K followed by monoclinic-to-hexagonal (or trigonal) transition at 1060 K [21]. The *P*2/*c*-*C*2/*m* phase transition can be explained by the fact that the *P*2/*c* space group is a Maximal klassengleiche subgroups of *C*2/*m* (n°12) as a result of the loss of centring translations [22]. In the case of $CaZr(PO_4)_2$, the structure was first shown to be orthorhombic ($P2_12_12_1$ space group) and totally different from the yavapaite one [12]. Recently, their crystal structure has been revised by ab initio Rietveld analysis of X-ray powder diffraction data [13]. The structure is shown to be orthorhombic with space group $Pna2_1$. A reversible second order transition was confirmed by high temperature XRD analysis and the space group is (*Pnma*, Z = 4). Results of single–crystal X-ray diffraction analysis show that both $SrM^{IV}(PO_4)_2$ (M = Ti, Sn) materials are isostructural and crystallise in a distorted yavapaiite-structure (*DY*) with monoclinic *C*2/*c* space group [14]. X-ray Rietveld analysis shows also that high-temperature β-$SrGe(PO_4)_2$ (*C*2/*m* space group) are isotypic with the true yavapaiite (*TY*) whereas the low-temperature α-$SrGe(PO_4)_2$ and the $CaGe(PO_4)_2$ (*C*2/c space group) are distorted derivatives [8]. In the same context note that the phase transition from *C*2/*c* to *C*2/*m*, which was reported for $SrGe(PO_4)_2$, is in good agreement with the fact that *C*2/*c* is a maximal klassengleiche subgroups of *C*2/*m* resulting from an enlargement of the unit cell [22]. Actinide barium phosphate, $BaAn^{IV}(PO_4)_2$ (An^{IV} = Th, Np) can also be seen as modified yavapaiite derivatives

with increased coordination numbers for Ba (XIV) and Th/Np (VIII) [23]. On the other hand, $SrNp(PO_4)_2$ structure is more related to cheralite than to yavapaiite [24].
Recently intensive research activities, realized by some of us, are particularly focused on characterization of phosphates belonging to the A-Sb-Fe-P-O (A = Mn, Ca, Cd, Sr, Pb) systems. Results of investigations led particularly to synthesis and characterization of a series of $A^{II}_{0.50}Sb^{V}Fe^{III}(PO_4)_3$ (A = Mn, Ca, Cd, Sr, Pb) Nasicon phases ($R\bar{3}$ space group). Structures of $A^{II}_{0.50}Sb^{V}Fe^{III}(PO_4)_3$ compounds show an ordered distribution of A^{II} ions in M1 sites and Sb^{V}/Fe^{III} ions within the Nasicon framework [15-18]. In our more recently reported works the phosphate $Ca^{II}_{1/3}Bi^{III}_{1/2}Sb^{V}_{1/6}PO_4$ which include a mixture of A^{II}, A'^{III} and A''^{V} ions has been isolated [25]. It crystallizes with the high temperature $BiPO_4$ monoclinic structure variety ($P2_1/m$ space group). So, in a continuation of our scientific search for new materials likely to exhibit interesting physical properties and belonging to the A-Sb-Fe-P-O systems, synthesis and structural characterisation of the three $A^{II}(Sb^{V}_{0.5}Fe^{III}_{0.5})(PO_4)_2$ (A = Ba, Sr, Pb) compounds are undertaken. In order to obtain further structural information about the nature of bonding in the crystalline solids, a Raman and Infrared spectroscopic study of selected phases is also presented.

II. Experimental

Syntheses of $A^{II}(Sb^{V}_{0.5}Fe^{III}_{0.5})(PO_4)_2$ (A = Ba, Sr, Pb) phases, abbreviated as [Ba], [Sr] and [Pb] respectively, were carried out using conventional solid-state reaction techniques. Powder crystalline samples were prepared from mixtures of Fe_2O_3 (Prolabo, 99 %), Sb_2O_3 (Riedel-de Haën, 99.9 %), $NH_4H_2PO_4$ (Riedel-de Haën, 99 %) and carbonates $SrCO_3$, $BaCO_3$ (Riedel-de Haën, 99 %) or nitrates $Pb(NO_3)_2$ (Prolabo, 99 %) in stoichiometric proportions. The mixtures were heated progressively with intermittent grinding at 200 °C (12 h), 600 °C (24 h), 750 °C (24 h) and 800 °C (48 h) in air. Additional treatments up to 850°C (48 h) are necessary for obtaining a pure sample. The products of reaction were characterised by X-ray diffraction (XRD) at room temperature with a Panalytical X'Pert-PRO (θ-2θ) diffractometer; (CuKα) radiation (45 kV, 40 mA). The data were collected over 8 h from 10 to 140° (2θ), in steps of 0.01313° for [Sr] and [Pb] phases and from 5 to 100° (2θ), in steps of 0.016711° for [Ba]. The Rietveld refinement of the structure was performed using the Fullprof program [26].
The infrared spectra were recorded in the form of KBr pellets in the wave number range 1500-400 cm^{-1} using a Bruker's VERTEX 70 spectrometer and the Raman spectra are recorded on RENISHAW 1000B spectrometer in the wave number range 50-1500 cm^{-1}. All the spectra have been recorded at room temperature.

3. Results and discussion

According to the literature data, peak positions and intensities of the XRPD patterns of $Ba(Sb_{0.5}Fe_{0.5})(PO_4)_2$ were close to those of the room temperature variety of $BaZr(PO_4)_2$ (*C2/m* space group, Z = 2) [6], therefore its XRPD patterns can be indexed, in a first approximation, on a similar monoclinic cell. In the case of the $A(Sb_{0.5}Fe_{0.5})(PO_4)_2$ (A = Sr, Pb) monophosphates, the peak positions and relative intensities of the XRPD patterns were almost similar to those of the yavapaiite $BaZr(PO_4)_2$ type-phase; however several additional weak extra reflections were observed.

3.1. Rietveld refinement and structural description of $Ba(Sb_{0.5}Fe_{0.5})(PO_4)_2$ phase

The Rietveld analysis in Le Bail's (profile matching) mode confirmed that [Ba] phase is compatible with the *C*2/*m* space group. So, initial starting parameters for the Rietveld refinement of $Ba(Sb_{0.5}Fe_{0.5})(PO_4)_2$ were based on those already reported by Fukuda et al. for the true yavapaiite (*TY*) $BaZr(PO_4)_2$ phase in the *C*2/*m* space group [6]. Soft constraints were applied to the P-O distances. This refinement leads to acceptable reliability factors. A comparison of the experimental and calculated XRD profile of [Ba] material is given in Figure 1. Results of the Rietveld refinement and selected interatomic distances are given in Tables 1 and 2 respectively. X-ray powder diffraction data, obtained from the ''observed intensities'' of the Rietveld refinement (CuKα1 : 1.540 56 Å), of [Ba] phase is presented in Table 3.

Structure of $Ba(Sb_{0.5}Fe_{0.5})(PO_4)_2$ consists of three types of polyhedra, BaO_{10}, PO_4 and $Sb(Fe)O_6$ (Fig. 2). It can also be viewed as being composed of alternating edge-sharing BaO_{10} bicapped square antiprism and $Sb(Fe)O_6$ octahedra forming chains parallel to c-axis (Fig. 2b). There are five chains per unit cell (Fig. 2a). Each $Sb(Fe)O_6$ octahedral is bound by its vertices to six PO_4 tetrahedra and shares two of its edges (i.e., O(3)-O(3) one) to two BaO_{10} polyhedra (Fig. 3a and 3b). The framework can be described as consisting of dense slabs of $Sb(Fe)O_6$ octahedra and PO_4 tetrahedra interconnected via corner-sharing, alternating along the c-axis with layers of Ba cations in ten-fold coordination (Fig. 2a and 2c). The ten oxygen atoms of each BaO_{10} polyhedron belong to six phosphate PO_4 groups. Eight of the oxygen atoms come from four bidentate PO_4 groups and the two other oxygens belong to the other two monodentate PO_4 groups (Fig. 3a and Fig. 3b). Projection onto ab plane of the structure of [Ba] compound shows that every BaO_{10} polyhedron is connected, via its O(1)-O(1) edges, to six neighbouring BaO_{10} polyhedra (Fig. 3c). The six neighbouring Ba-Ba distances values vary between 4.836(3) Å and 5.200(3) Å. In fact, within each BaO_{10} polyhedron, the Ba-O distances values can divide to two groups (Table 2). The first group contains six relatively shortest Ba-O distances with values varying between 2.75 and 2.83 Å whereas the second group is formed by four longest Ba-O distances with a value of 3.11 Å. Therefore, the coordinence of Ba atoms in $Ba(Sb_{0.5}Fe_{0.5})(PO_4)_2$ can be considered as 6+4. Obtained Sb(Fe)-O interatomic distances are consistent with the crystal radii values in six coordination of Sb^{5+} and Fe^{3+} ions [27]. Note that the similarity of the crystal radii of Fe^{3+} (0.785 Å, HS) and Sb^{5+} (0.74 Å) ions is in favor of their distribution in the same site. P-O distances values match well with those typically observed in phosphates and the O-P-O angles vary between 105 and 118°. In order to have more structural information, the bond valence sum (BVS) based on bond strength analysis [28] for $Ba(Sb_{0.5}Fe_{0.5})(PO_4)_2$ were also computed. As shown in Table 2, the BVS values calculated for Ba, Fe, Sb and P sites are relatively consistent with the expected formal oxidation state of Ba^{2+}, Fe^{3+}, $Sb^{5+}$and P^{5+} ions.

3.2. Rietveld refinement and structural description of $A(Sb_{0.5}Fe_{0.5})(PO_4)_2$ (A = Sr, Pb) phases

An attempt to refine the diffraction patterns of the $A(Sb_{0.5}Fe_{0.5})(PO_4)_2$ (A = Sr, Pb) compounds with the known (*TY*) $BaZr(PO_4)_2$ structural model (*C2/m* space group) yielded to anomalous high reliability factors and intensity residuals. Figure 4a gives, for example, a comparison between observed, calculated, and difference XRD patterns of [Pb] in the 10-35° (2θ range). Note that several small peaks which are indicated by a vertical arrow at the vicinity of 2θ° equal to 18, 25, 28 and 29 remain unindexed. In fact, in the case of $PbSb_{0.5}Fe_{0.5}(PO_4)_2$ [Pb], this last refinement gives values of the unit-cell parameters (a_{TY} = 8.121 Å, b_{TY} = 5.181 Å, c_{TY} = 7.587 Å,

β_{TY} = 94.0° and V_{TY} = 319 Å^3) which are relatively comparable to those obtained for the (*TY)* $Ba(Sb_{0.5}Fe_{0.5})(PO_4)_2$.

In the following section, the indexing of the [Sr] and [Pb] XRPD patterns was performed by means of the computer program DICVOL [29]. The first 40 peak positions, with a maximal absolute error of 0.02° (2θ), were used as input data. For each phase, four monoclinic cells were found but only one result corresponding to a satisfactory figure of merit [29] is retained for the next stages of refinements. Note, for example, that in the case of $Pb(Sb_{0.5}Fe_{0.5})(PO_4)_2$ the obtained unit-cell parameters are a = 8.121 Å; b = 5.181 Å, c = 15.152 Å, β = 94.0° and V = 636 Å^3. The corresponding figures of merit are (M20/F20 = 146.5/236.9(0.0013, 65) and (F(31) = 48.7(0.0015, 434)). A careful analysis of this last result shows that the unit cell volume (V = 636 Å^3) is doubled as result of the doubling of the lattice parameter c in the *DY* (Distorted Yavapaiite) (ie.: a_{DY} = a_{TY} = 8.121 Å, b_{DY} =b_{TY} = 5.181 Å, c_{DY} = 2×c_{TY} = 15.152 Å, and β_{DY} = 94.0°). Until this stage of refinement, we can admit the existence of a group subgroup relationship between the space group of [Pb] and that of the *C*2/*m* space group of the *TY*. This last group-subgroup relation is a consequence direct of the enlargement of the unit cell [22]. The Check-Group program, which is integrated within the *Fullprof-suite* program [30], has been used to obtain the ordered list of possible space groups (*see details in [Pb]Cell choice 3.spg as supplementary information file*). Among the thirteen possible space groups (ie. *I*12/*a*1(n°15), *I*1*a*1(n°9), *I*121(n°5), *I*1*m*1(n°8), *I*12/*m*1(n°12), $P12_1/c1$(n°14), *P*1*c*1 (n°7), *P*12/*c*1(n°13), $P12_11$ (n°4), $P12_1/m1$(n°11), *P*12/*m*1 (n°10), *P*1*m*1(n°6), *P*121(n°3)), the *I*2/*a* (n°15) was found with the satisfactory merit factors. Given that *I*12/*a*1 (cell choice 3) is not a standard space group, the cell edges of the doubled-cell *DY* in the standard *C*2/*c* (n°15) space group (cell choice 1) can be deduced by the following vectorial relations (a_1 = -a_3-c_3, b_1 = b_3, c_1 = a_3) (Fig. 5) [31]. Calculated values of the derived unit-cell parameters, in the standard *C*2/*c* space group, are a_1 = 16.681 Å; b_1 = 5.183 Å, c_1 = 8.121 Å and β_1 = 115.04°. By using the following vectorial relations (a_2 = -a_1-c_1, b_2 = b_1, c_2 = a_1), values of the cell parameters in the non-standard A2/n (n°15) space groups (cell choice 2) can also be easily deduced (Fig. 5) (ie. a_2 = 15.152 Å, b_2 = 5.181 Å, c_2 = 16.681 Å and β_2 = 150.96°). In order to reverified the correctness of the choice of the standard space group (cell choice 1), the use of Check-Group program with the unit-cell parameters of a_1, b_1, c_1 and β_1 = 115.04° was performed (*see details in [Pb]Cell choice 1.spg as supplementary information file*). The results show that among the thirteen possible space groups only the *Cc* (n°9) and *C*2/*c* (n°15) space groups were found with the satisfactory merit factors (Table 4). Results of the Le Bail fitting (profile matching) program [32], realized in both *Cc* and *C*2/*c* space group for the [Sr] and [Pb] materials, show comparable and lower reliability factors. Comparison between observed and calculated XRD patterns obtained from the Le Bail fitting program of $Pb(Sb_{0.5}Fe_{0.5})(PO_4)_2$, in the 10-35° (2θ range), is given in figure 4b. As it will be shown later, the unindexed reflections in figure 4a appear as the $h+l = 2n+1$ superstructure reflections of a *C*2/*c* doubled cell similar to that obtained by Zhao et al. for $SrTi(PO_4)_2$ [14]. Note that among the two possible *Cc* and *C*2/*c* space groups, the choice of structural refinement in the high-symmetry *C*2/*c* space group seems to be the most probable.

In the succeeding step of Rietveld refinement, the initial starting structural parameters were based on those already reported for $SrTi(PO_4)_2$ phase (*C*2/*c* space group). The A and Sb(Fe) atoms in $A(Sb_{0.5}Fe_{0.5})(PO_4)_2$ phases are supposed to occupy respectively the two special 4e (0, -y, 3/4) and 4c (1/4, 1/4, 0) Wyckoff positions whereas the P, and O atoms are located in the general 8f Wyckoff positions. During the Rietveld

refinement, a soft constraint were applied to the P-O distances and anisotropic thermal factors for Pb atoms in $Pb(Sb_{0.5}Fe_{0.5})(PO_4)_2$ phase are also used. For both [Sr] and [Pb] phases, the last hypothesis of structural refinement led to lower reliability factors (Tables 5 and 6). Observed, calculated, and difference XRD patterns of both compounds are shown in Figures 6 and 7. Selected interatomic distances of [Sr] and [Pb] phases are gathered in Tables 7 and 8 respectively. X-ray powder diffraction data, obtained from the ''observed intensities'' of the Rietveld refinement (CuKα1 : 1.540 56 Å), of both phases are given in Tables 9 and 10.

Given that [Sr] and [Pb] compounds are isomorphous, only the structure of $Sr(Sb_{0.5}Fe_{0.5})(PO_4)_2$ will be discussed in detail as a representative. $Sr(Sb_{0.5}Fe_{0.5})(PO_4)_2$ is a 3D diorthophosphate which crystallises in a distorted yavapaiite structure-type. In fact, although the [Sr] phase has a *C*2/*c* space group and their *a*-parameter is the double in comparison to that of $Ba(Sb_{0.5}Fe_{0.5})(PO_4)_2$, both materials have a similar 3D network. The structure of [Sr] can be described as constructed by alternating $[(Sb_{0.5}Fe_{0.5})(PO_4)_2]^{2-}$ anionic sheets and Sr^{2+} cationic sheets along the [101] direction (Fig. 8). The Sr^{2+} sheets reside among those of $[(Sb_{0.5}Fe_{0.5})(PO_4)_2]^{2-}$ sheets alternatively and join them through Coulombic action of Sr^{2+} cations and O^{2-} anions to form the 3D framework of $Sr(Sb_{0.5}Fe_{0.5})(PO_4)_2$. The Sr atom is coordinated by ten oxygen atoms from six PO_4 tetrahedra (two of them in a unidentate fashion and four of them in edge-sharing fashion) (Fig. 8b). Careful analysis of the A-O distances (A = Sr, Pb) within AO_{10} polyhedron of [Sr] and [Pb] compounds shows that A atom is surrounded by eight oxygen atoms with 'normal' bond distances (2.585(2)-2.792(2) Å for [Sr] and 2.651(3)-2.697(2) Å for [Pb]) and two oxygen atoms with 'abnormal' bond distances (3.448(2) Å for [Sr] and 3.546(3) Å for [Pb]) (Tables 7 and 8). Therefore, the coordinence of A atoms in both $A(Sb_{0.5}Fe_{0.5})(PO_4)_2$ (A = Sr, Pb) phases can be considered as 8+2. In all cases A-O distances values (A = Sr, Pb) are comparable with those of the Sr-O and Pb-O ones which are already obtained for $SrTi(PO_4)_2$ and $PbTi(PO_4)_2$ materials [14,33]. Within the Sr^{2+} cationic sheets every SrO_{10} polyhedron is connected, via its O(4)-O(4) edges, to six neighbouring SrO_{10} polyhedra (Fig. 8c). The six neighbouring Sr-Sr distance values vary between 4.536(3) Å and 5.189(3) Å. In [Pb] phase, the corresponding Pb-Pb distances, within the Pb^{2+} cationic sheets, are ranging between 4.510(3) Å and 5.518(3) Å. The dispersion of A-A distances (A = Sr, Pb) values is in close relation with the connection mode between the AO_{10} polyedra. Every $Sb(Fe)O_6$ octahedron is interconnected *via* common corners (O(1), O(2) and O(3) atoms) to six PO_4 tetrahedra and shares two of its edges (i.e., O(1)-O(2) one) to two SrO_{10} polyhedra (Fig. 8b). Obtained Sb(Fe)-O interatomic distances are consistent with the crystal radii values in six coordination of Sb^{5+} and Fe^{3+} ions (Tables 7 and 8) [27]. P-O distances values match well with those typically observed in orthophosphates. In order to have more structural information, the bond valence sum (BVS) [28] for $A(Sb_{0.5}Fe_{0.5})(PO_4)_2$ (A = Sr, Pb) phases were also computed. As shown in Tables 7 and 8, the BVS values calculated for A, Fe, Sb and P sites are relatively consistent with the expected formal oxidation state of A^{2+}, Fe^{3+}, $Sb^{5+}$and P^{5+} ions.

It is of interest to note that our attempts to synthesize $CaSb_{0.5}Fe_{0.5}(PO_4)_2$ was not satisfactory, although identical synthesis conditions have been applied. Indeed analysis of the obtained XRD spectra shows principally the presence of a mixture of the already known $Ca_{0.50}SbFe(PO_4)_3$ Nasicon phase and two $Ca_2P_2O_7$ (PDF number 81-2257) and $SbOPO_4$ (PDF number 84-830) phosphates which are identified as minority phases [16,34,35]. Our experimental result shows that $[Sb_{0.5}Fe_{0.5}(PO_4)_2]^{2-}$ yavapaiite framework appears well adapted to bigger Sr^{2+}, Pb^{2+} and Ba^{2+} cations.

This last result agrees with the recent report by some of us about the relationships between composition and crystal structure [20]. Indeed we can conclude that for alkaline earth metal cations of smaller and/or equal size than the Ca^{2+} ions, the $[SbFe(PO_4)_3]^-$ Nasicon framework seems to be the more stable.

3.3 Raman spectroscopy

Raman and Infrared spectroscopic study was undertaken in order to obtain further structural information about the nature of bonding in $A(Sb_{0.5}Fe_{0.5})(PO_4)_2$ (A = Sr, Pb) phases. Given that the yavapaiite structure contains both isolated PO_4 groups and isolated $Sb(Fe)O_6$ groups, the vibrational pattern is obviously typical of an orthophosphate. Note that the vibrational modes of tetrahedral PO_4 molecules are well known [36]. Generally the IR and Raman spectroscopic study of orthophosphate shows that phosphate group vibrations are strong compared to the lattice modes and metal-oxygen vibrations. The IR and Raman band positions of the four (ν_1, ν_2, ν_3 and ν_4) modes observed in the spectra of the [Sr] and [Pb] phases (Figs. 9 and 10) are close to those expected for yavapaiite phosphate type materials [37]. Thus, the symmetric non degenerate PO stretching modes (ν_1) are observed in the range 920-1040 cm^{-1} while antisymmetric doubly degenerate PO stretching (ν_2) are located in the 430-480 cm^{-1} range. The symmetric, triply degenerate OPO bending (ν_3) is observed between 1070-1170 cm^{-1} and the triply degenerate, antisymmetric and harmonic OPO bending (ν_4) is observed in the range 540-650 cm^{-1}.
The Sb-O…P bonds existing in both compounds have an average length of 2.00 Å. Their stretching vibrations are probably coupled with the O-P-O bending ν_4 mode. As was already observed for $SbOPO_4$ phase [38], the frequencies found between 575 and 650 cm^{-1} in Raman and Infrared spectra of [Sr] and [Pb] phases can be assigned empirically to Sb-O stretching modes involving Sb-O-P linkage. In the lattice modes region, the translational modes of Sr^{2+} or Pb^{2+}, Fe^{3+}, Sb^{5+} and PO_4^{3-} ions as well as librational modes of PO_4^{3-} ions and FeO_6, SbO_6 groups should be expected. At wavenumbers below 450 cm^{-1} strong coupling between the different bending vibrations O-P-O, O-Sb-O, Sb-O-P is expected [39]. The Raman bands observed at 364 and 370 cm^{-1} could be assigned to Fe^{3+}-O stretching modes of vibrations similar to those observed in $Li_3Fe_2(PO_4)_3$ [40]. The low frequency modes observed below 270 cm^{-1} can be easily attributed to translational modes of the Sr^{2+}or Pb^{2+}, Fe^{3+}, Sb^{5+} and $(PO_4)^{3-}$ ions.

Conclusion

A new family of double phosphate with general formula $A^{II}(Sb^{V}_{0.5}Fe^{III}_{0.5})(PO_4)_2$ (A = Ba, Sr, Pb) were prepared by solid state reaction method and caracterised from X-ray powder diffraction using the Rietveld method. Note that phases with a mixing of Sb^{V} and Fe^{III} ions in the octahedral M sites of the $A^{II}M^{IV}(PO_4)_2$ yavapaiite structure-types were studied here for the first time. $Ba(Sb^{V}_{0.5}Fe^{III}_{0.5})(PO_4)_2$ features the yavapaiite-type structure, with space group *C*2/*m*. $Sr(Sb^{V}_{0.5}Fe^{III}_{0.5})(PO_4)_2$ and $Pb(Sb^{V}_{0.5}Fe^{III}_{0.5})(PO_4)_2$ crystallize in monoclinic system with space group *C*2/*c* (distorted yavapaiite type structure). The $[(Sb_{0.5}Fe_{0.5})(PO_4)_2]^{2-}$ yavapaiite framework appears well adapted to bigger Sr^{2+}, Pb^{2+} and Ba^{2+} cations. Contrary to these last results, for smaller alkaline earth metal cations as Ca^{2+}, the $[SbFe(PO_4)_3]^-$ Nasicon framework seems to be the more stable. Further investigations on the relationships between composition and crystal structure, as well as research on potential application of phases of general formula $A^{II}(M^{V}_{0.5}B^{III}_{0.5})(PO_4)_2$ were in progress.

References

[1] N. Clavier , R. Podor, N. Dacheux, J. Eur. Ceram. Soc., 31 (2011**)** 941–976.
[2] D. B. Kitaev, Y. F. Volkov, A. I. Orlova, Radiochemistry, 46(3) (2004) 211-217
[3] A. I. Orlova**,** D. B. Kitaev, N.G. Kazantsev, S.G Samoilov, V.S. Kurazhkovskaya, E.N. Vopilina, Radiochemistry, 4 (2002) 326–331
[4] A. I. Orlova**,** D. B. Kitaev, D. V. Kemenov, M. P. Orlova, G. N. Kazantsev, S. G. Samoilov, V. S.Kurazhkovskaya, Radiochemistry, 45 (2003)103-109.
[5] J. J. Finney, N. Nagaraja Rao, Am. Mineral. 1967, 52, 13-19.
[6] K. Fukuda, A. Moriyama, T. Iwata, J. Solid State Chem., 178 (2005) 2144-2151.
[7] K. Popa, D. Bregiroux, J. M. Konnings, T.Gouder, Aurelian F. Popa, T. Geisler, E. P. Raison, J. Solid State Chem.,180 **(**2007**)** 2346-2355.
[8] K. Popa, G. Wallez , D. Bregiroux, P. Loiseau, J. Solid State Chem., 184 (2011) 2629-2634.
[9] A. Leclaire, M. M. Borel, J. Chardon, B. Raveau, J. Solid State Chem., 116 (1995) 364-368.
[10] E. Morin, G. Wallez, S. Jaulmes, J. C. Couturier, M. Quarton, J. Solid State Chem., 137 (1998) 283–288
[11] K. Fukuda, A. Moriyama, S. Hashimoto, J. Solid State Chem., 177 (2004) 3514–3521.
[12] K. Fukuda, K. Fukutani, Powder Diffr. 18 (2003) 296-300.
[13] D. Bregiroux, G. Wallez, K. Popa, Solid State Sciences 41 (2015) 43-47.
[14] D. Zhao, H. Zhang, Z. Xie , W.L. Zhang, S.L. Yang, W.D. Cheng, Dalton Trans., 27 (2009) 5310-5318.
[15] A. Aatiq, R. Hassine, R. Tigha, I. Saadoune, Powder Diffr., 20 (2005) 33-39
[16] A. Aatiq, R. Tigha, R. Hassine, I. Saadoune, Powder Diffr., 21 (2006) 45–51
[17] A. Aatiq, R. Tigha, S. Benmokhtar, J. Mater. Sci., 47(3) (2012) 1354-1364.
[18] A. Aatiq, R. Tigha, R. Fakhreddine, A. Marchoud, J. Mater. Environ. Sci. 6 (12) (2015) 3483-3490.
[19] D. Bregiroux, K. Popa, R. Jardin, P.E. Raison, G. Wallez, M. Quarton, M. Brunelli, C. Ferrero, R. Caciuffo, J. Solid State Chem. 182 (2009) 1115-1120.
[20] D. Bregiroux, K. Popa, G. Wallez, J. Solid State Chem., 230 (2015) 26–33.
[21] K. Fukuda, T. Iwata, A. Moriyama, S. Hashimoto, J. Solid State Chem., 179 (2006) 3870-3876.
[22] International Tables for Crystallography Vol. A1: Symmetry relation between space group, Editors Hans Wondratschek and Ulrich Müller. First Ed., Published by Kluwer Academic Publishers, Dordrecht/Boston/London (2004) page 106.
[23] G. Wallez, D. Bregiroux, K. Popa, P.E. Raison, C. Apostolidis, P. Lindqvist-Reis, R.J.M. Konings, A.F. Popa, Eur. J. Inorg. Chem. (2011) 110-115.
[24] K. Popa, G. Wallez, P.E. Raison, D. Bregiroux, C. Apostolidis, P. Lindqvist-Reis, R.J.M. Konings, Inorg. Chem. 49 (2010) 6904-6908.
[25] A. Aatiq, R. Tigha, Powder Diffr., 29 (2014) 14-19.
[26] J. Rodriguez-Carvajal, (1990). Collected Abstracts of Powder Diffraction Meeting, (Toulouse, France), 127.
[27] R. D. Shannon, Acta Crystallogr., Sect.A: Cryst. Phys., Diffr., Theor. Gen. Crystallogr., 32 (1976) 751-767
[28] I. D. Brown, D. Altermatt, Acta Crystallogr., Sect. B: Struct. Sci. B41 (1985) 244-247.
[29] A. Boultif ,D. Louër, J. Appl. Cryst., 37 (2004) 724-731.
[30] J. Rodriguez-Carvajal, FULLPROF.2k : Rietveld, Profile Matching and Integrated Intensity Refinement of X-ray and Neutron Data, V 1.9c, Laboratoire Leon

Brillouin, CEA, Saclay, France, 2001.
[31] International Tables for Crystallography Vol. A: Space-Group Symmetry, Editor Theo Hahn. Fifth ed., Published by Springer, (2005) pages : 22, 192–195.
[32] A. Le Bail, H. Duroy, J.L. Fourquet, Mat. Res. Bull., 23 (1988) 447-452
[33] W.-L. Zhang, C.-S. Lin, Z.-Z. He, H. Zhang, Z.-Z. Luo, W.-D. Cheng, Cryst. Eng. Comm., 15 (2013) 7089-7094
[34] S. Boudin, A. Grandin, M. M. Borel, A. Leclaire, B. Raveau, Acta Crystallogr. Sec. C., 49 (1993) 2062-2064.
[35] Y. Piffard**,** S. Oyetola, A. Verbaere, M. Tournoux, J. Solid State Chem., 63 (1986) 81-85.
[36] K. Nakamoto, Infrared and Raman Spectra of Inorganic and Coordination Compounds, fourth ed., Wiley–Interscience, New York, 1986, p. 138.
[37] M.Th. Paques-Ledent, J. Inorg. Nucl. Chem. 39(1) (1977) 11-17.
[38] V. Sudarsan, K. P. Muthe, J.C. Vyas, S.K. Kulshreshtha, J. Alloys Compd., 336 (2002) 119-123.
[39] E. Husson, F. Genet, A. Lachgar, Y. Piffard, J. Solid State Chem., 75 (1988) 305-312.
[40] G. Butt, N., Sammes, G. Tompsett, A. Smirnova, O. Yamamoto, J. Power sources, 134 (2004) 72-79.

Figures captions

Figure 1. Experimental (•••) calculated (—), and difference profile of the XRD pattern of $Ba(Sb_{0.5}Fe_{0.5})(PO_4)_2$.
Figure 2. View of the structure of $Ba(Sb_{0.5}Fe_{0.5})(PO_4)_2$ (a); rows of BaO_{10}, PO_4 and $Sb(Fe)O_6$ polyhedra along c-axis (b) and projection in the ac plane (c).
Figure 3. Array of BaO_8 polyhedra in (*a*) and (b); view of $BaO_8(BaO_8)_6$ polyhedra in (c) within the structure of $Ba(Sb_{0.5}Fe_{0.5})(PO_4)_2$.
Figure 4. Experimental (•••) calculated (—), and difference profile of the XRD pattern, in the 10-35° (2θ range), of $Pb(Sb_{0.5}Fe_{0.5})(PO_4)_2$ with refinement in *C*2/*m* in (a) and *C*2/*c* in (b). Unindexed peaks are indicated by a vertical arrow.
Figure 5. View along the b-axis of the three Monoclinic space groups C2/c (cell choice 1), A2/n (cell choice 2) and I2/a (cell choice 3). The unique b-axis points upwards from the page and the subscripts of the labels of the axes indicate the cell choice.
Figure 6. Experimental (•••) calculated (—), and difference profile of the XRD pattern of $Sr(Sb_{0.5}Fe_{0.5})(PO_4)_2$.
Figure 7. Experimental (•••) calculated (—), and difference profile of the XRD pattern of $Pb(Sb_{0.5}Fe_{0.5})(PO_4)_2$.
Figure 8. Projection of the structure of $Sr(Sb_{0.5}Fe_{0.5})(PO_4)_2$ in the ac plane (a); rows of polyhedra along a-axis (b) and $SrO_8(SrO_8)_6$ polyhedra (c)
Figure 9. Raman spectra of $Sr(Sb_{0.5}Fe_{0.5})(PO_4)_2$ (a) and $Pb(Sb_{0.5}Fe_{0.5})(PO_4)_2$ (b).
Figure 10. I R. Spectra of of $Sr(Sb_{0.5}Fe_{0.5})(PO_4)_2$ (a) and $Pb(Sb_{0.5}Fe_{0.5})(PO_4)_2$ (b).

Tables captions
Table 1. Results of the Rietveld refinement of $Ba(Sb_{0.5}Fe_{0.5})(PO_4)_2$.
Table 2. Selected interatomic distances and calculated Bond valence sum (BVS) for $Ba(Sb_{0.5}Fe_{0.5})(PO_4)_2$.
Table 3. Powder diffraction data of $Ba(Sb_{0.5}Fe_{0.5})(PO_4)_2$ (Cu$K\alpha_1$; λ = 1.5406 Å)

Table 1. Results of the Rietveld refinement of $Ba(Sb_{0.5}Fe_{0.5})(PO_4)_2$.

$Ba(Sb_{0.5}Fe_{0.5})(PO_4)_2$
Space group, *C*2/*m* (N°12); [Z = 2; a = 8.1568(4) Å; b = 5.1996(3) Å c = 7.8290(4) Å; β = 94.53(1) °; V = 331(1) $Å^3$]
Profile parameters
Pseudo-Voigt function, PV = ηL + (1-η)G; η = 0.27(1)
Half-width parameters, U = 0.126(4), V = 0.012(3), and W = 0.010(1)
Conventional Rietveld R-factors, R_{WP} = 9.6%; R_P = 6.9%; R_B = 3.9%; R_F = 2.6%

Atom	Site	Atomic coordinates			$B_{iso}(Å^2)$	Occupancy
Ba	2c	0	0	0.5	1.3(1)	1
(Sb,Fe)	2a	0	0	0	0.5(1)	0.5/0.5
P	4i	0.3645(2)	0	0.2024(3)	0.8(1)	1
O(1)	4i	0.3111(6)	0	0.3871(4)	0.7(1)	1
O(2)	4i	0.2309(6)	0	0.0516(6)	0.7(1)	1
O(3)	8j	0.4766(5)	0.2351(5)	0.1833(5)	0.7(1)	1

Table 2. Selected interatomic distances and calculated Bond valence sum (BVS) for $Ba(Sb_{0.5}Fe_{0.5})(PO_4)_2$.

$Ba(Sb_{0.5}Fe_{0.5})(PO_4)_2$		
Sb(Fe)-O distances (Å)	P-O distances (Å)	Ba-O distances (Å)
2×Sb(Fe)-O(2) = 1.895(5)	P-O(1) = 1.543(4)	2×Ba-O(1) = 2.752(6)
4×Sb(Fe)-O(3) = 2.009 (3)	P-O(2) = 1.542(5)	4×Ba-O(3) = 2.829(4)
Aver.<Sb(Fe)-O> = 1.95(1)	2×P-O(3) = 1.541(4)	4×Ba-O(1) = 3.114(3)
	Aver. <P-O> = 1.54(1)	Aver. <Ba-O> = 2.92(1)
Bond Valence Sums (BVS)		
BVS(Sb(Fe)) = 4.7 (should be 4)	BVS (P) = 4.9	BVS (Ba) = 1.8

Table 3. Powder diffraction data of $Ba(Sb_{0.5}Fe_{0.5})(PO_4)_2$ (Cu$K\alpha_1$; λ = 1.5406 Å)

hkl	d_{obs} (Å)	100 I/I_0 (obs)	100 I/I_0 (cal)	*hkl*	d_{obs} (Å)	100 I/I_0 (obs)	100 I/I_0 (cal)
001	7.8045	4	4	132	1.5455	6	5
110	4.3805	100	90	-422	1.5150	6	5
200	4.0656	60	69	-224	1.4887	5	4
002	3.9023	33	31	-512	1.4811	3	3
-111	3.8913	30	30	314	1.4654	4	5
111	3.7524	33	33	-404	1.4667	4	4
-201	3.7284	21	21	330	1.4602	7	6
201	3.4944	3	4	422	1.4502	5	6
-112	2.9774	85	78	224	1.4271	2	1
-202	2.9334	10	10	512	1.4063	2	3
112	2.8541	50	50	-332	1.3871	1	1
202	2.7104	9	10	600	1.3552	2	2
020	2.5998	30	28	332	1.3489	1	1
310	2.4035	34	36	040	1.3000	3	3
-311	2.3437	1	1	-134	1.2902	2	2
-203	2.2744	3	2	134	1.2693	2	2
311	2.2531	2	2	-116	1.2617	5	4
220	2.1903	5	4	240	1.2382	1	1
022	2.1636	18	17	042	1.2333	1	1
-221	2.1326	7	6	206	1.2114	2	1
-312	2.1136	14	12	424	1.2017	3	3
400	2.0328	5	6	530	1.1859	1	1
312	1.9853	6	6	-316	1.1791	1	1
004	1.9511	16	14	514	1.1724	3	2
222	1.8762	9	9	043	1.1628	1	1
-402	1.8642	4	4	-425	1.1542	2	1
-313	1.8304	3	3	334	1.1459	2	2
-204	1.8159	9	9	532	1.1169	1	1
-114	1.8112	11	10	316	1.1118	2	2
114	1.7548	7	7	440	1.0951	2	2
402	1.7472	6	9	044	1.0818	1	1
130	1.6951	4	3	712	1.0668	2	1
131	1.6509	1	1	-244	1.0569	2	1
420	1.6014	2	2	-534	1.0403	3	2
-132	1.5642	8	8	800	1.0164	1	1
510	1.5521	5	5				

[a] Diffraction lines with I_{obs}< 1 are omitted.

Table 4. Ordered list of possible space groups obtained from the Check-Group program for $Pb(Sb_{0.5}Fe_{0.5})(PO_4)_2$

Space-groups number	Hermann-Mauguin Symbol of space groups	Merit factors
9	*C* 1 *c* 1	2.70
15	*C* 1 2/*c* 1	2.70
5	*C* 1 2 1	1.97
8	*C* 1 *m* 1	1.97
12	*C* 1 2/*m* 1	1.97
14	*P* 1 2_1/*c* 1	1.38
7	*P* 1 *c* 1	1.35
13	*P* 1 2/*c* 1	1.35
4	*P* 1 2_1 1	1.01
11	*P* 1 2_1/*m* 1	1.01
10	*P* 1 2/*m* 1	1.00
6	*P* 1 *m* 1	1.00
3	*P* 1 2 1	1.00

Table 5. Results of the Rietveld refinement of $Sr(Sb_{0.5}Fe_{0.5})(PO_4)_2$.

$Sr(Sb_{0.5}Fe_{0.5})(PO_4)_2$						
Space group, *C*2/*c* (N°15); [Z = 4; a = 16.5215(2) Å; b = 5.1891(1) Å c = 8.0489(1) Å; β = 115.70(1)°; V = 622(1) $Å^3$						
Profile parameters						
Pseudo-Voigt function, PV = ηL + (1-η)G; η = 0.384(3)						
Half-width parameters, U = 0.0122(2), V = -0.0054(2), and W = 0.0045(1)						
Conventional Rietveld R-factors, R_{WP} = 4.1%; R_P = 2.8%; R_B = 4.3%; R_F = 2.6%						
Atom	Site	Atomic coordinates			$B_{iso}(Å^2)$	Occupancy
Sr	4e	0	0.2985(1)	0.75	1.0(1)	1
(Sb,Fe)	4c	0.25	0.25	0	0.14(1)	0.5/0.5
P	8f	0.1431(1)	0.7579(3)	0.7588(1)	0.45(2)	1
O(1)	8f	0.1449(2)	1.0196(5)	0.8615(5)	0.22(3)	1
O(2)	8f	0.1591(2)	0.5270(5)	0.8954(4)	0.22(3)	1
O(3)	8f	0.2219(2)	0.7647(6)	0.7067(4)	0.22(3)	1
O(4)	8f	0.0498(2)	0.7225(6)	0.6017(4)	0.22(3)	1

Table 6. Results of the Rietveld refinement of $Pb(Sb_{0.5}Fe_{0.5})(PO_4)_2$.

$Pb(Sb_{0.5}Fe_{0.5})(PO_4)_2$

Space group, *C*2/*c* (N°15); [Z = 4; a = 16.6925(2) Å; b = 5.1832(1) Å c = 8.1215(1) Å; β = 115.03(1)°; V = 637(1) $Å^3$]

Profile parameters

Pseudo-Voigt function, PV = ηL + (1-η)G; η = 0.438(4)

Half-width parameters, U = 0.048(1), V = -0.008(1), and W = 0.005(1)

Conventional Rietveld R-factors, R_{WP} = 4.1%; R_P = 6.1%; R_B = 4.5%; R_F = 3.1%

Atom	Site	Atomic coordinates			$B_{iso}(Å^2)$	Occupancy
Pb	4e	0	0.3106(7)	0.75	-----	1
(Sb,Fe)	4c	0.25	0.25	0	0.06(1)	0.5/0.5
P	8f	0.1455(3)	0.7587(6)	0.7626(2)	0.57(5)	1
O(1)	8f	0.1444(2)	1.0213(6)	0.8636(3)	0.07(1)	1
O(2)	8f	0.1612(3)	0.5326(6)	0.9013(3)	0.07(1)	1
O(3)	8f	0.2212(7)	0.7634(4)	0.7049(6)	0.07(2)	1
O(4)	8f	0.0520(2)	0.7107(5)	0.6090(5)	0.07(2)	1

Anisotropic Betas×10^4	B_{11}	B_{22}	B_{33}	B_{12}	B_{13}
Pb	18.8(0.5)	76.4(3.1)	202.8(2.6)	0	35.7(0.9)

Table 7. Selected interatomic distances and calculated Bond valence sum (BVS) for $Sr(Sb_{0.5}Fe_{0.5})(PO_4)_2$.

$Sr(Sb_{0.5}Fe_{0.5})(PO_4)_2$		
Sb(Fe)-O distances (Å)	P-O distances (Å)	Sr-O distances (Å)
2×Sb(Fe)-O(1) = 2.002(3)	P-O(1) = 1.583(3)	2×Sr-O(1) = 2.601(3)
2×Sb(Fe)-O(2) = 1.982(3)	P-O(2) = 1.569(3)	2×Sr-O(2) = 2.650(3)
2×Sb(Fe)-O(3) = 1.913(4)	P-O(3) = 1.532(4)	2×Sr-O(4) = 2.585(3)
Aver.<Sb(Fe)-O> = 1.97(1)	P-O(4) = 1.522(3)	2×Sr-O(4) = 2.792(3)
	Aver. <P-O> = 1.55(1)	2×Sr-O(4) = 3.448(3)
		Aver. <Sr-O> = 2.65(1)
Bond Valence Sums (BVS)		
BVS(Sb(Fe)) = 4.4 (should be 4)	BVS (P) = 4.8	BVS (Sr) = 1.9

Table 8. Selected interatomic distances and calculated Bond valence sum (BVS) for $Pb(Sb_{0.5}Fe_{0.5})(PO_4)_2$.

$Pb(Sb_{0.5}Fe_{0.5})(PO_4)_2$		
Sb(Fe)-O distances (Å)	P-O distances (Å)	Pb-O distances (Å)
2×Sb(Fe)-O(1) = 2.022(5)	P-O(1) = 1.593(6)	2×Pb-O(1) = 2.651(6)
2×Sb(Fe)-O(2) = 1.995(5)	P-O(2) = 1.569(6)	2×Pb-O(2) = 2.697(6)
2×Sb(Fe)-O(3) = 1.920(8)	P-O(3) = 1.522(9)	2×Pb-O(4) = 2.684(6)
Aver.<Sb(Fe)-O> = 1.98(1)	P-O(4) = 1.552(5)	2×Pb-O(4) = 2.669(5)
	Aver. <P-O> = 1.55(1)	2×Pb-O(4) = 3.546(6)
		Aver. <Pb-O> = 2.67(1)
Bond Valence Sums (BVS)		
BVS(Sb(Fe)) = 4.3 (should be 4)	BVS (P) = 4.8	BVS (Pb) = 1.8

Table 9. Powder diffraction data of $Sr(Sb_{0.5}Fe_{0.5})(PO_4)_2$ (Cu$K\alpha_1$; λ = 1.5406 Å)

hkl	d_{obs} (Å)	100 I/I_0 (obs)	100 I/I_0 (cal)	*hkl*	d_{obs} (Å)	100 I/I_0 (obs)	100 I/I_0 (cal)
200	7.4435	10	9	-912	1.7301	4	4
110	4.9000	4	4	602	1.7280	19	16
-111	4.3591	58	56	-804	1.7254	14	15
-202	4.0174	54	53	-623	1.7214	1	1
111	3.8154	28	26	130	1.7182	2	1
400	3.7217	19	18	-911	1.6919	15	14
-311	3.7099	19	17	-131	1.6910	5	5
002	3.6263	11	10	-913	1.6741	1	1
310	3.5864	3	3	422	1.6642	3	2
-402	3.4509	16	17	131	1.6534	6	5
-312	3.0774	2	2	-10 02	1.6516	3	3
311	2.8765	100	100	330	1.6333	2	2
202	2.8146	6	7	114	1.6266	1	1
-511	2.7865	74	75	223	1.6098	1	2
-602	2.6529	10	11	-821	1.5970	1	1
020	2.5946	39	40	-424	1.5883	3	2
510	2.5825	3	3	-132	1.5837	1	1
600	2.4812	4	3	-332	1.5759	1	1
021	2.4430	3	3	-224	1.5684	2	1
-313	2.3799	67	69	331	1.5468	11	10
221	2.2268	4	4	-515	1.5350	8	9
312	2.2250	3	3	-531	1.5323	7	7
-421	2.1946	5	5	132	1.5235	1	1
511	2.1868	3	3	820	1.5122	8	7
-222	2.1795	1	1	513	1.5049	5	4
420	2.1284	32	30	-532	1.5029	1	1
-711	2.1271	6	6	530	1.4956	1	1
-712	2.1233	2	2	10 00	1.4887	3	3
002	2.1101	4	3	-715	1.4868	3	3
-422	2.0738	2	2	024	1.4862	18	16
-802	2.0572	3	3	-333	1.4530	10	9
113	2.0548	17	16	-115	1.4483	4	4
-404	2.0087	14	15	622	1.4382	11	11
-713	1.9588	9	9	-824	1.4367	15	15
421	1.9178	1	1	-11 13	1.4299	10	10
222	1.9077	22	19	332	1.4155	1	1
-621	1.8838	2	2	404	1.4073	2	2
800	1.8609	13	12	531	1.4055	1	1
-223	1.8586	2	2	-11 11	1.3952	2	1
-622	1.8549	18	16	-10 22	1.3933	3	2
-514	1.8460	1	1	-915	1.3916	4	4
-423	1.8398	1	1	-731	1.3893	1	1
004	1.8131	8	7	133	1.3685	2	2
620	1.7932	2	1	224	1.3671	2	2
023	1.7687	3	3	-10 21	1.3628	1	1
313	1.7646	3	3	730	1.3419	1	1
711	1.7317	9	8	115	1.3398	1	1
-606	1.3391	4	4	-12 24	1.1811	3	3
-12 04	1.3265	1	2	-535	1.1773	3	3
-10 24	1.3101	3	3	-641	1.1725	1	1
-534	1.3013	1	1	-243	1.1663	1	1
040	1.2973	4	4	-14 02	1.1660	5	5
713	1.2931	1	1	-642	1.1654	1	1
532	1.2873	1	1	533	1.1634	1	1
-206	1.2845	1	1	-735	1.1551	1	1
240	1.2780	1	1	-13 15	1.1525	2	2
041	1.2770	1	1	-226	1.1512	5	5

-241	1.2750	1	1	-11 33	1.1278	3	3
731	1.2593	1	1	913	1.1246	2	2
-931	1.2438	2	2	206	1.1188	1	1
12 00	1.2406	1	1	-935	1.1087	1	1
-242	1.2345	1	1	10 22	1.0934	1	1
-13 13	1.2333	1	1	-841	1.0926	1	1
315	1.2185	8	7	-317	1.0907	1	1
-442	1.2143	2	2	-444	1.0898	1	1
10 02	1.2057	1	1	804	1.0846	1	1
11 11	1.2034	6	6	-15 13	1.0771	1	1
-626	1.1900	2	2	840	1.0642	2	1
-13 11	1.1832	1	1	-14 22	1.0636	3	3

[a] Diffraction lines with $I_{obs} < 1$ are omitted.

Table 10. Powder diffraction data of $Pb(Sb_{0.5}Fe_{0.5})(PO_4)_2$ ($CuK\alpha_1$; λ = 1.5406 Å)

hkl	d_{obs} (Å)	100 I/I_0 (obs)	100 I/I_0 (cal)	*hkl*	d_{obs} (Å)	100 I/I_0 (obs)	100 I/I_0 (cal)
200	7.5625	5	5	-804	1.7357	7	9
110	4.9033	13	13	-623	1.7262	3	2
-111	4.3661	99	92	130	1.7166	5	5
-202	4.0508	61	69	-911	1.7116	12	11
400	3.7812	37	34	-131	1.6897	3	2
-311	3.7210	49	44	-10 02	1.6691	3	3
002	3.6795	29	22	131	1.6542	1	1
310	3.6140	11	9	114	1.6497	1	1
-112	3.1583	3	3	-331	1.6440	2	2
-312	3.0888	4	5	330	1.6344	4	4
311	2.9131	100	100	223	1.6261	1	1
202	2.8658	14	14	-821	1.6089	2	2
-511	2.8065	77	78	-424	1.5959	2	2
112	2.7665	2	2	-132	1.5850	3	3
-602	2.6726	14	18	-332	1.5760	3	2
-512	2.6321	2	3	-823	1.5572	2	2
510	2.6126	5	5	331	1.5511	6	5
020	2.5916	26	30	-515	1.5465	6	6
600	2.5208	10	9	-521	1.5344	4	3
021	2.4444	8	8	-10 04	1.5277	9	7
-221	2.4279	7	7	-532	1.5039	3	2
-313	2.3950	51	56	530	1.5003	11	9
-113	2.3251	3	2	-115	1.4661	3	3
312	2.2585	5	4	622	1.4566	9	8
-513	2.2436	5	5	-11 13	1.4412	11	12
221	2.2358	8	7	404	1.4329	1	1
402	2.2107	3	2	332	1.4230	2	2
-421	2.1985	11	10	-11 11	1.4128	2	2
-222	2.1831	5	4	821	1.4031	4	3
-711	2.1483	2	2	-915	1.3991	2	3
420	2.1377	28	25	-732	1.3913	2	1
022	2.1188	6	5	133	1.5757	2	2
113	2.0825	16	15	730	1.3494	3	3
-802	2.0762	7	10	-12 04	1.3363	1	1
-404	2.0254	10	11	-334	1.3147	1	1
710	1.9944	1	1	-534	1.3044	1	1
-713	1.9689	10	10	-206	1.3007	1	1
421	1.9327	4	3	040	1.2958	2	2
222	1.9222	17	13	-134	1.2863	1	1
800	1.8906	12	12	-11 15	1.2807	1	1
-223	1.8668	3	3	041	1.2762	2	2
-622	1.8605	16	13	-241	1.2738	2	2
-423	1.8449	4	3	-932	1.2638	1	1
004	1.8397	6	5	12 00	1.2604	1	1
313	1.7927	4	4	-734	1.2581	1	1
023	1.7815	5	4	-931	1.2509	1	1
602	1.7610	17	16	-735	1.1587	1	1
241	1.2435	1	1	-11 32	1.1392	1	1
-441	1.2370	4	4	12 20	1.1335	2	1
11 11	1.2233	4	3	-643	1.1306	1	1
-442	1.2140	1	1	641	1.1063	1	1
930	1.2047	1	1	-11 34	1.1010	1	1
-626	1.1975	1	1	-841	1.0957	1	1
-934	1.1861	2	2	-15 13	1.0879	1	1
-535	1.1819	2	2	-843	1.0789	1	1
-14 02	1.1803	2	2	-14 22	1.0742	2	1
-641	1.1738	1	1	733	1.0690	1	1

732	1.1708	1	1	12 21	1.0612	1	1
-243	1.1675	1	1				
-443	1.1621	2	2				

[a] Diffraction lines with I_{obs}< 1 are omitted.

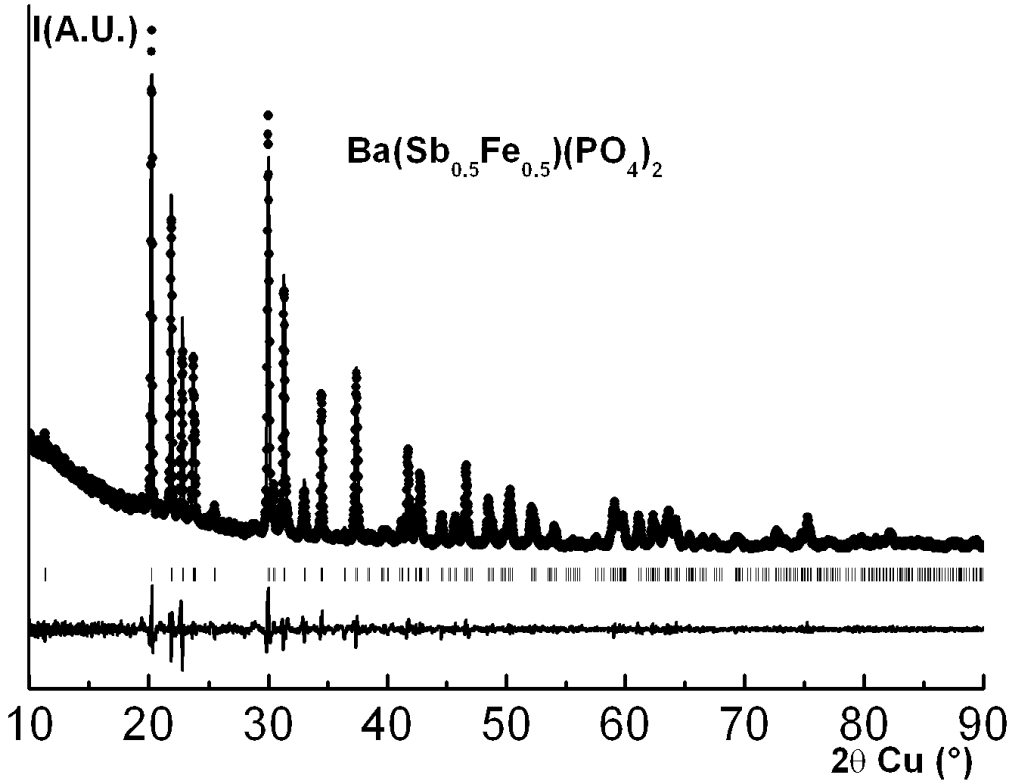

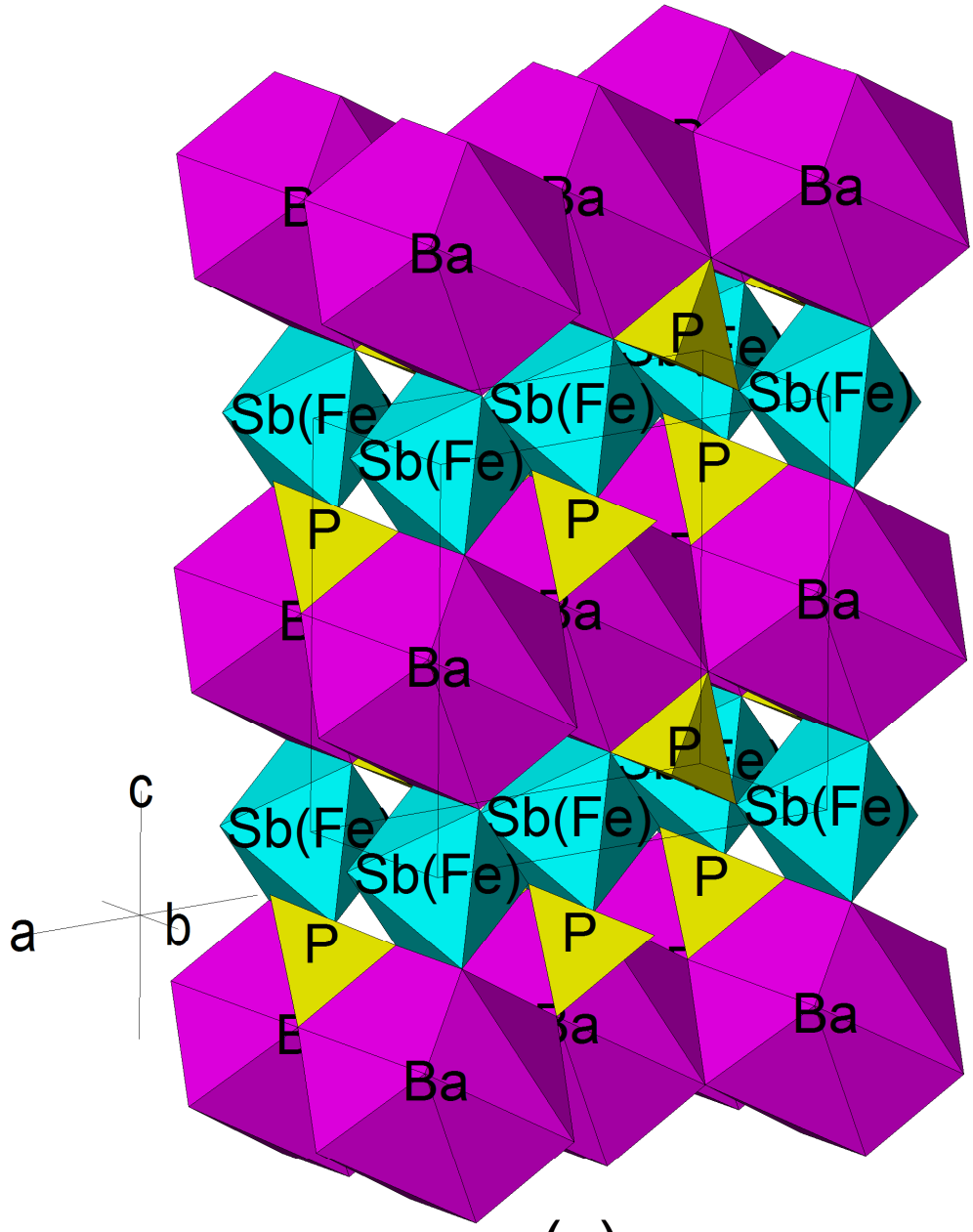

(a)

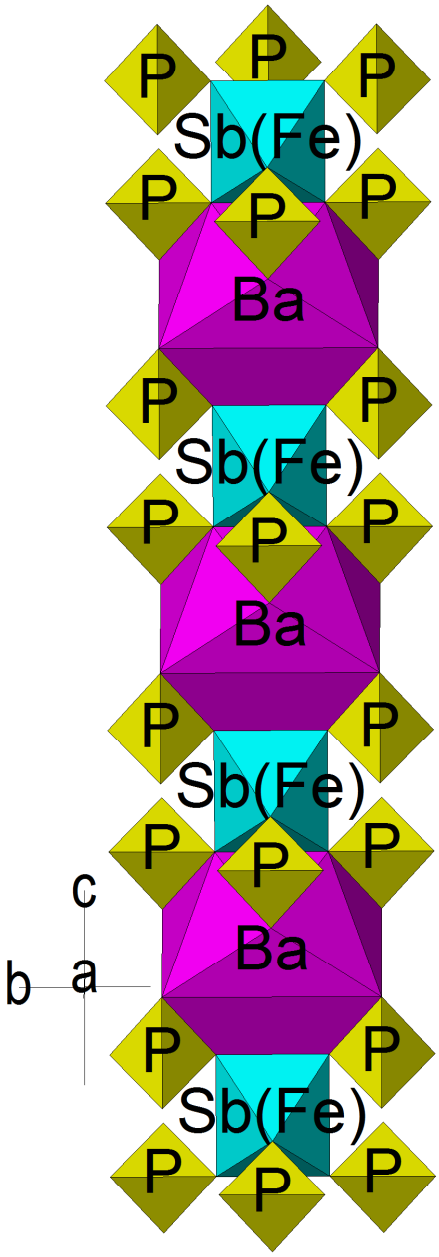

(b)

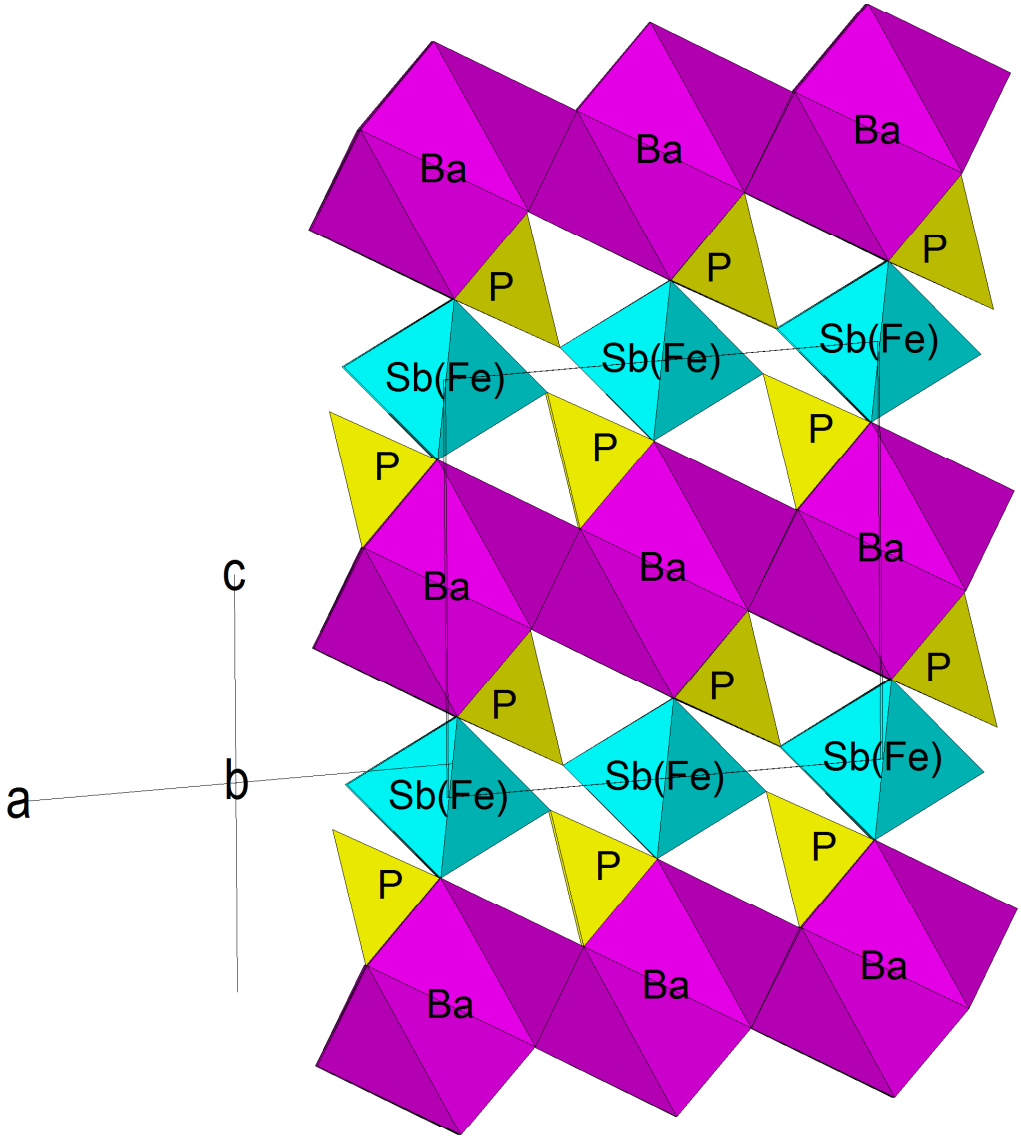
Ba
Ba
Ba
P
P
P
Sb(Fe)
Sb(Fe)
Sb(Fe)
P
P
P
Ba
Ba
Ba
P
P
P
Sb(Fe)
Sb(Fe)
Sb(Fe)
P
P
P
Ba
Ba
Ba
c
b
a

(c)

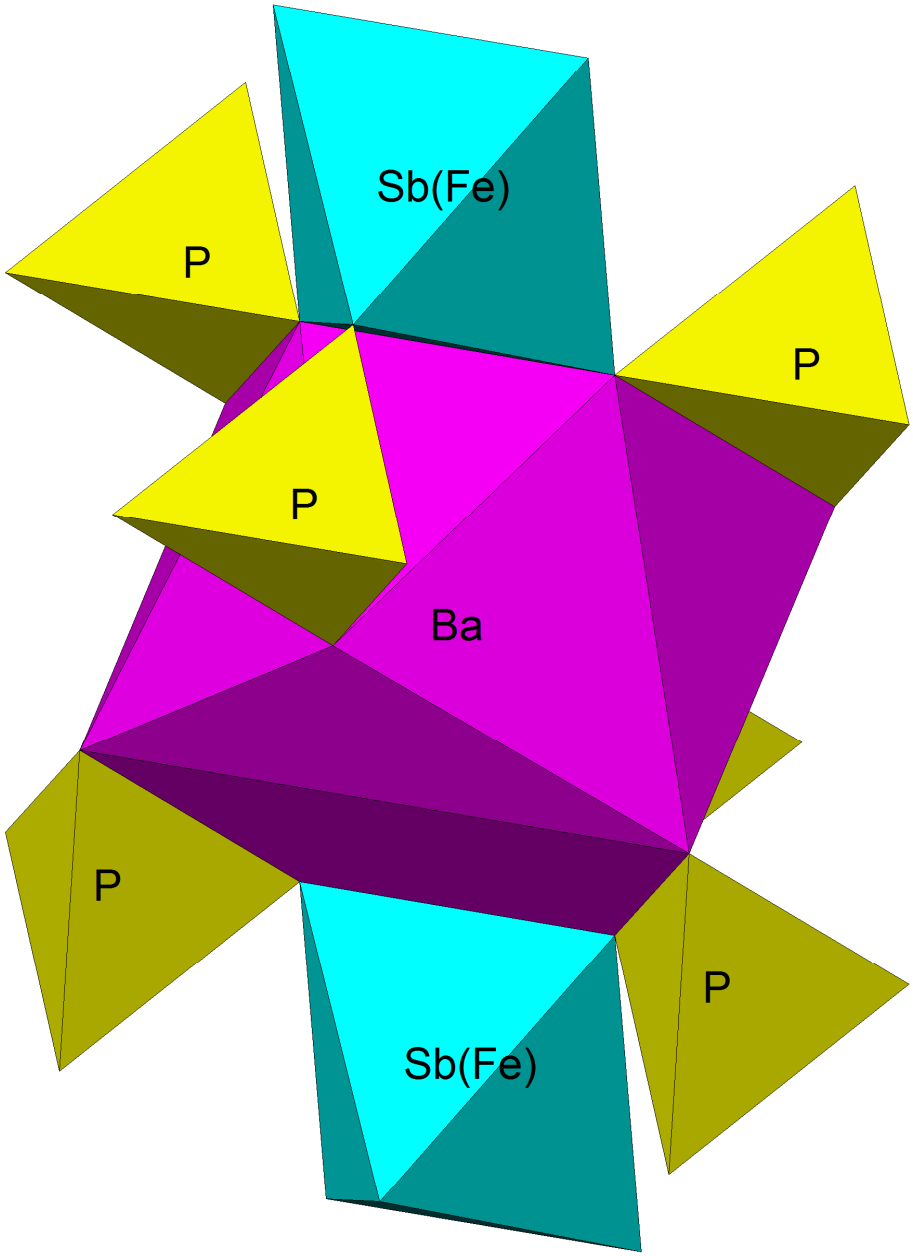

(a)

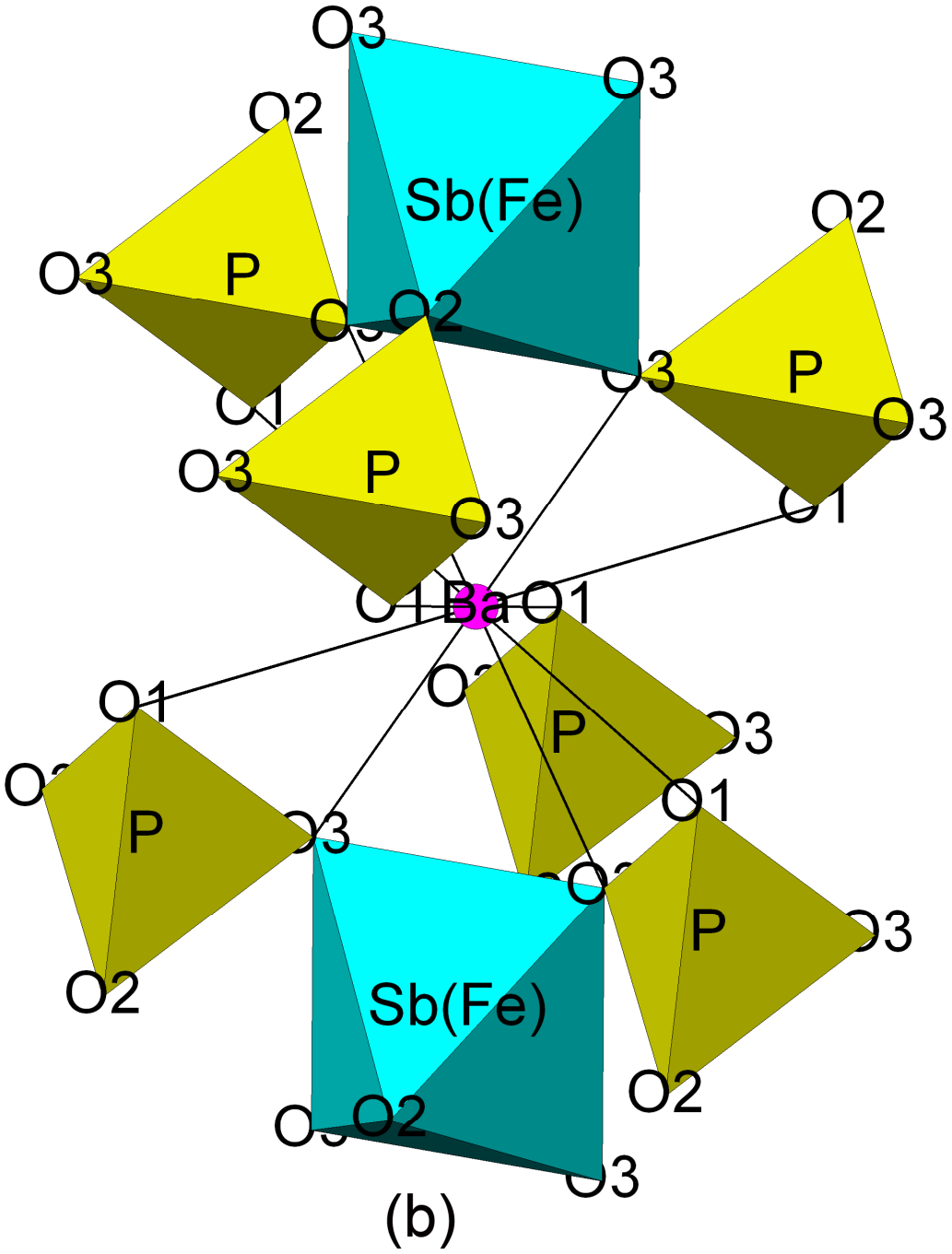
O3
O3
O2
Sb(Fe)
O2
O3
P
O2
O3
P
O3
O1
O3
P
O3
O1
Ba
O1
O1
P
O3
O1
P
O3
O1
P
O3
O2
Sb(Fe)
O2
O3

(b)

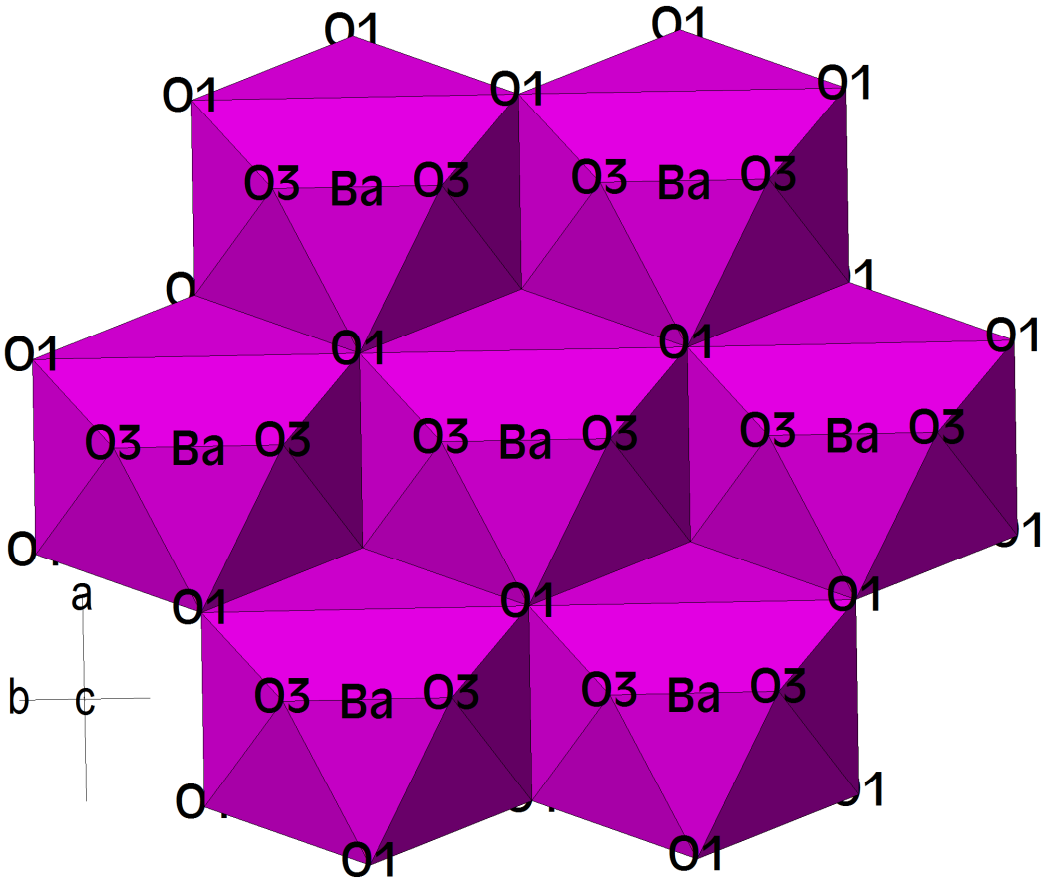

(c)

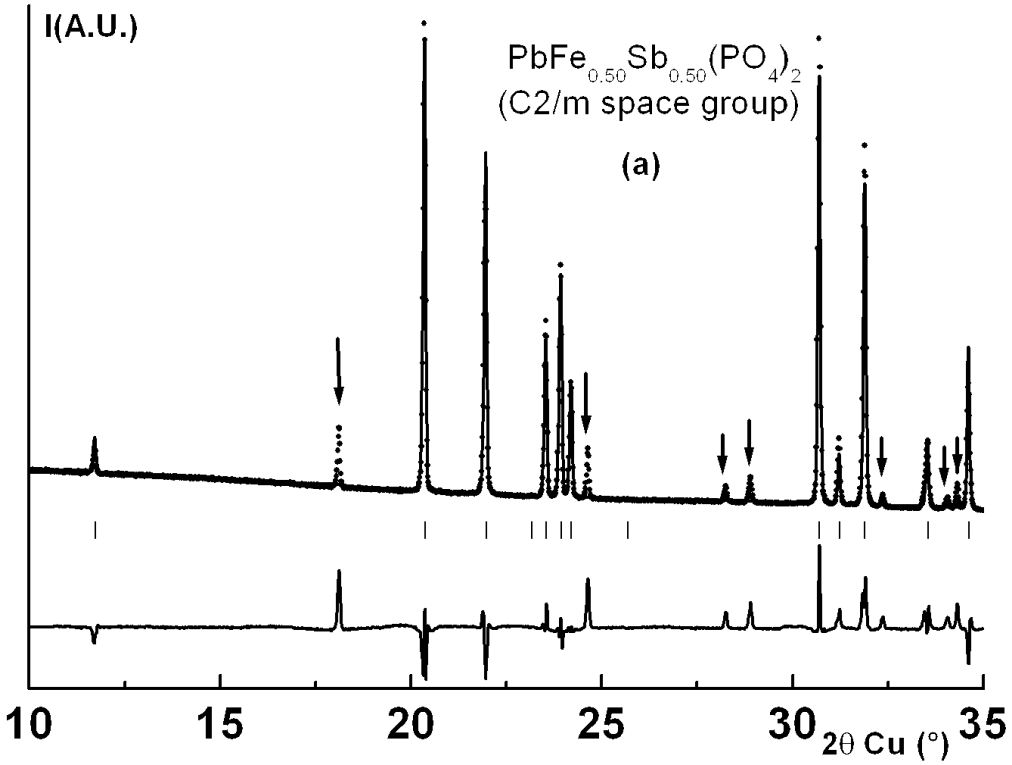

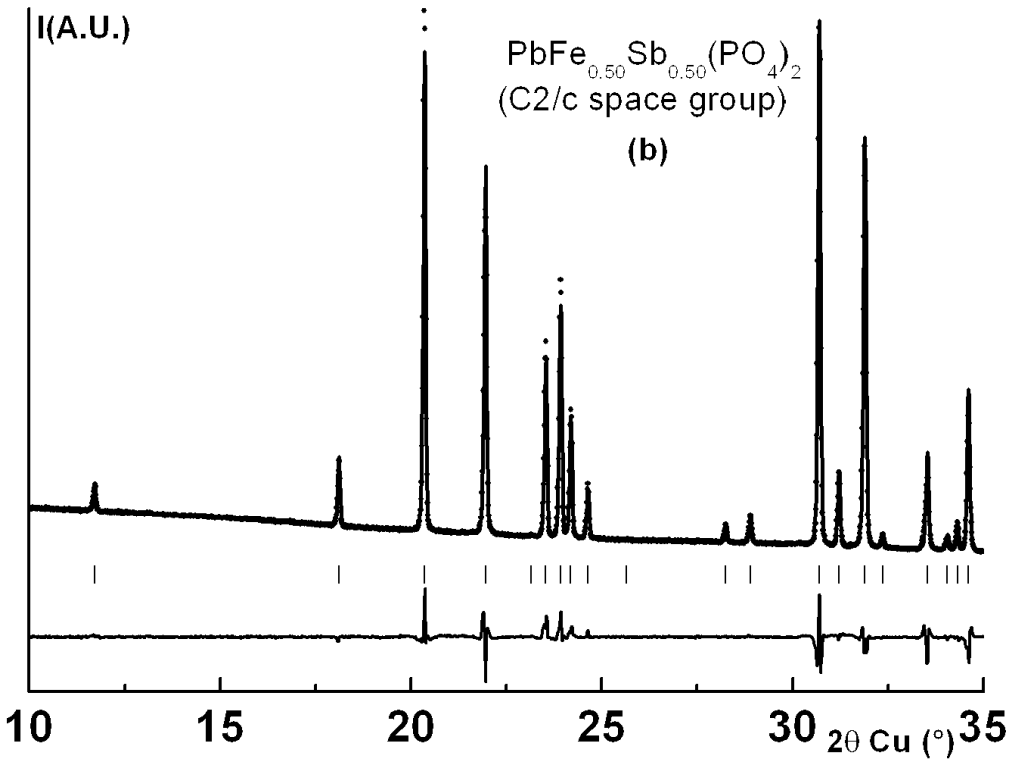

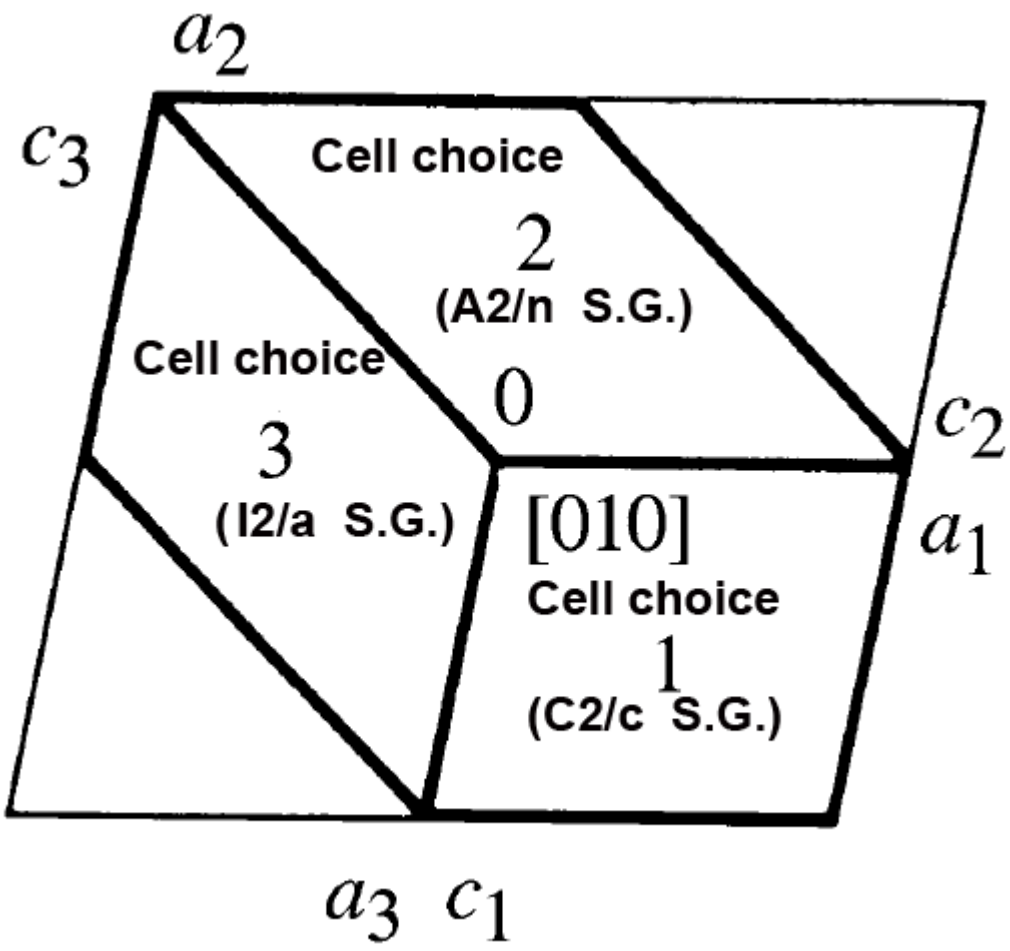
a_2
c_3
Cell choice
2
(A2/n S.G.)
Cell choice
0
3
(I2/a S.G.)
c_2
[010]
a_1
Cell choice
1
(C2/c S.G.)
a_3 c_1

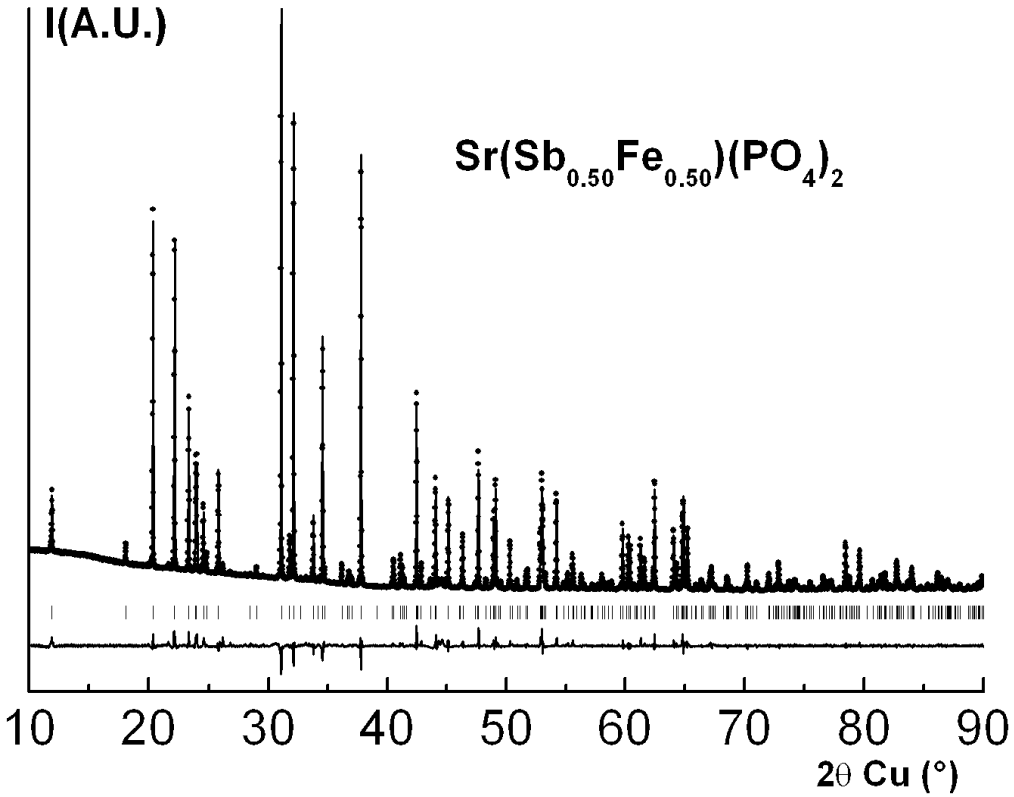

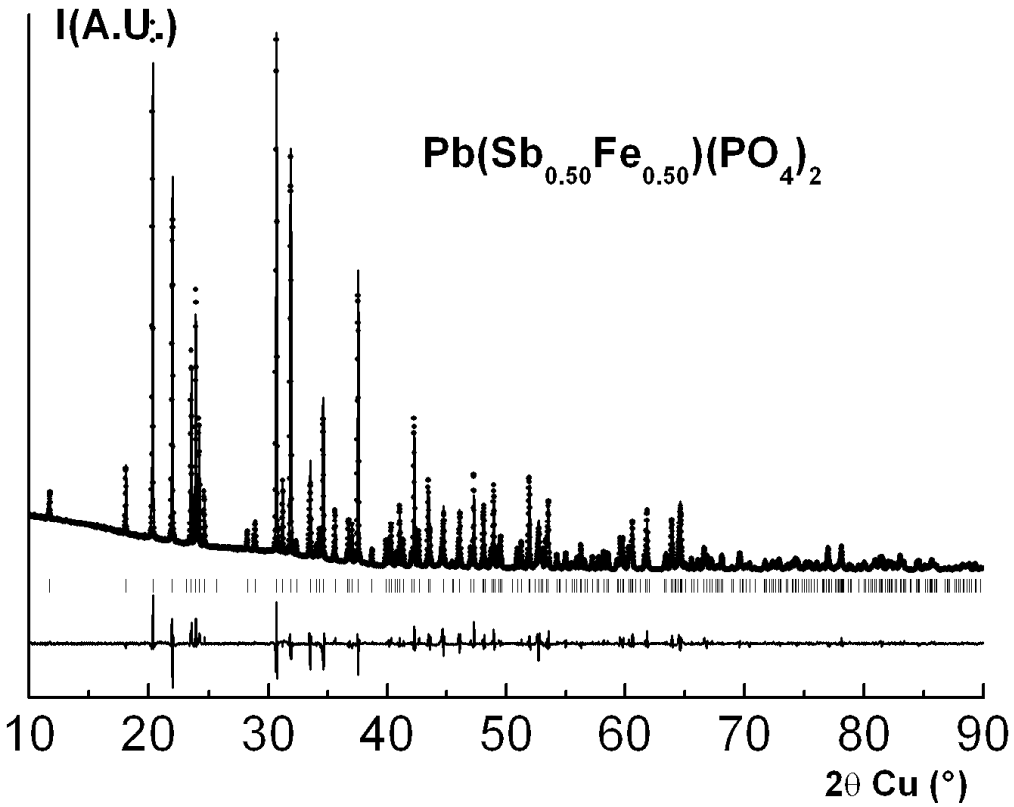

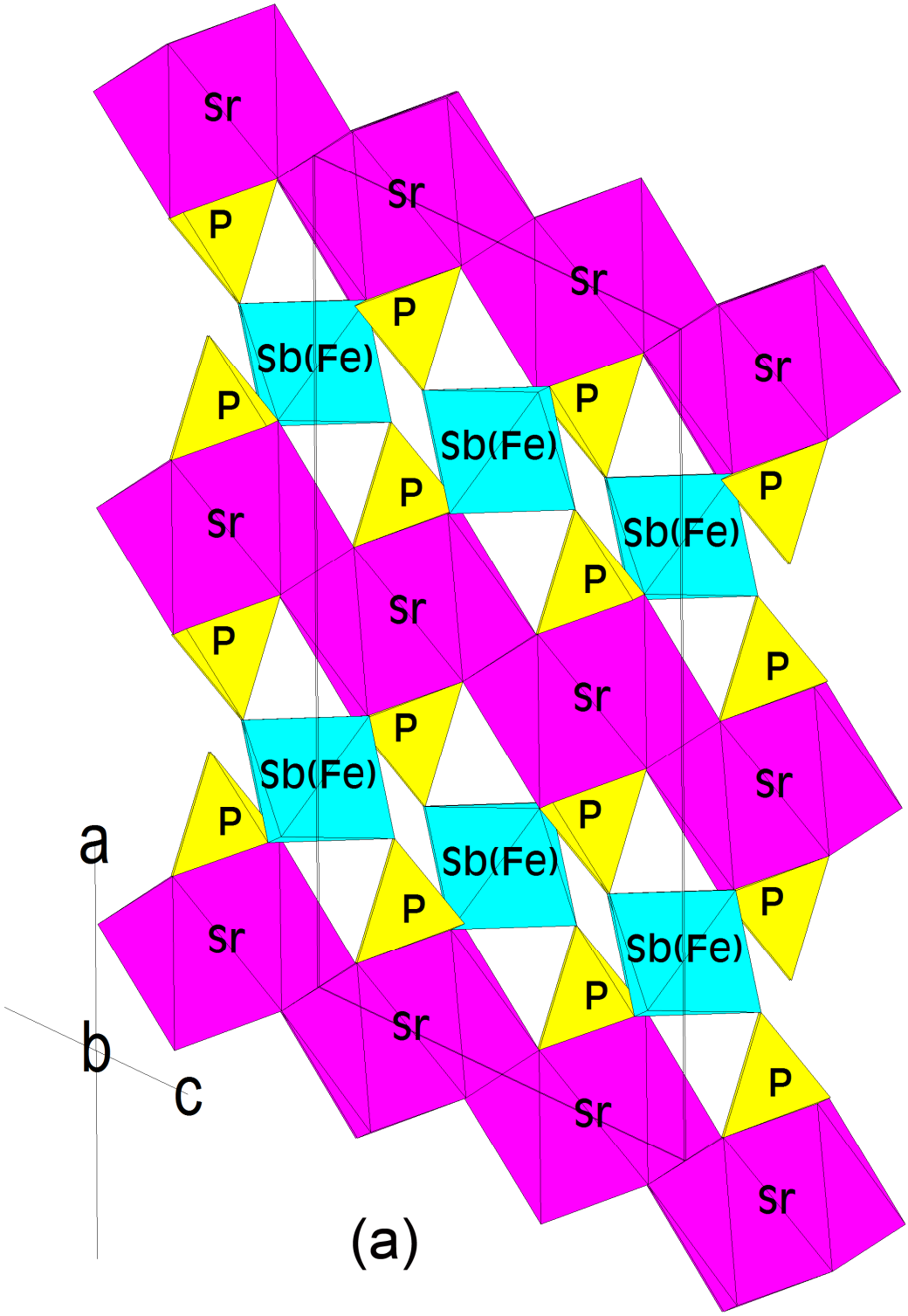
Sr
P
Sb(Fe)
a
b
c
(a)

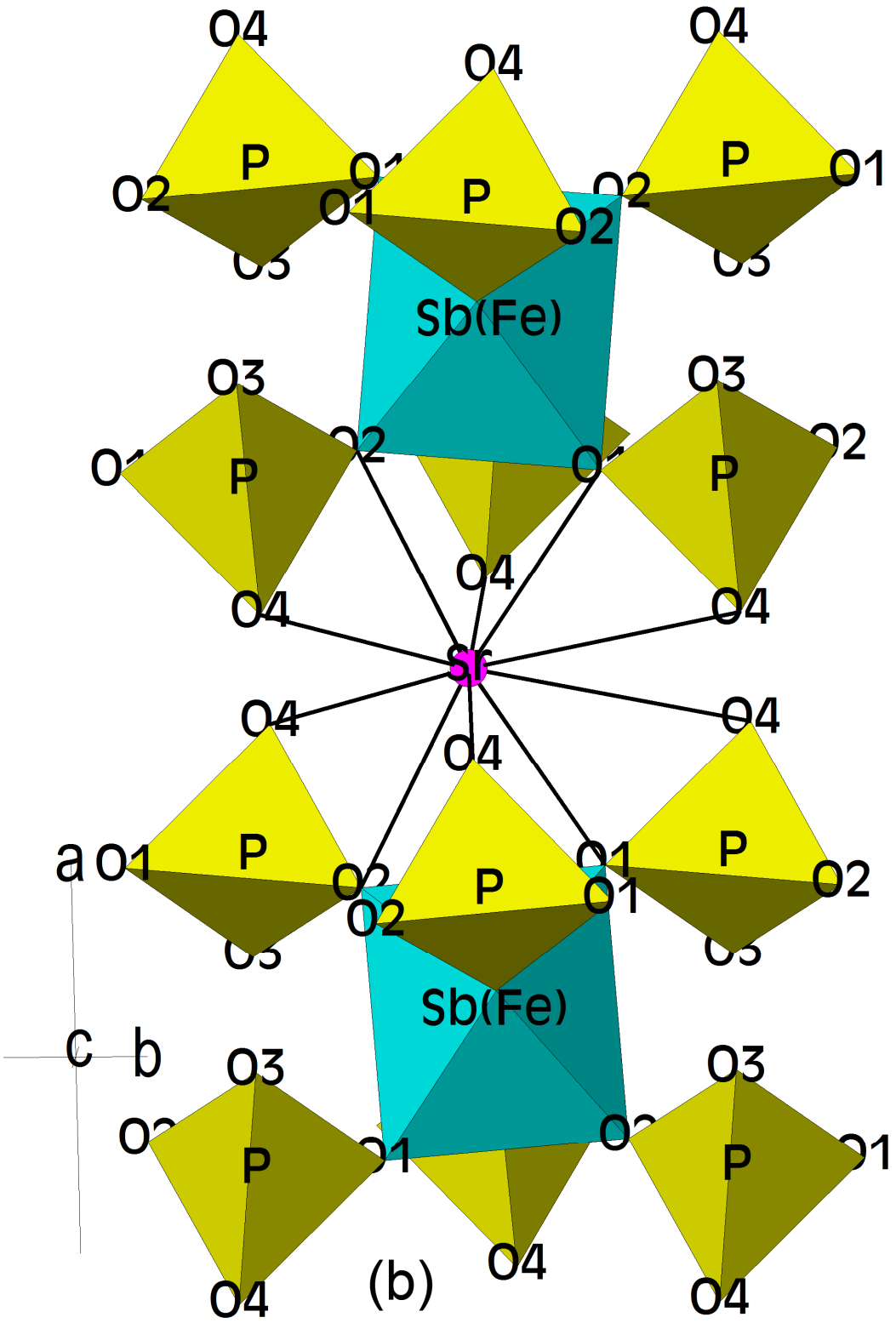
O4
O4
O4
P
O2
O1
O1
P
O2
P
O1
O2
O3
O3
Sb(Fe)
O3
O3
O1
O2
O2
P
P
O4
O4
O4
Sr
O4
O4
O4
a
O1
P
O2
O1
P
O1
P
O2
O2
O3
O3
Sb(Fe)
c
b
O3
O3
O2
O2
P
P
O1
O1
O4
O4
O4
(b)

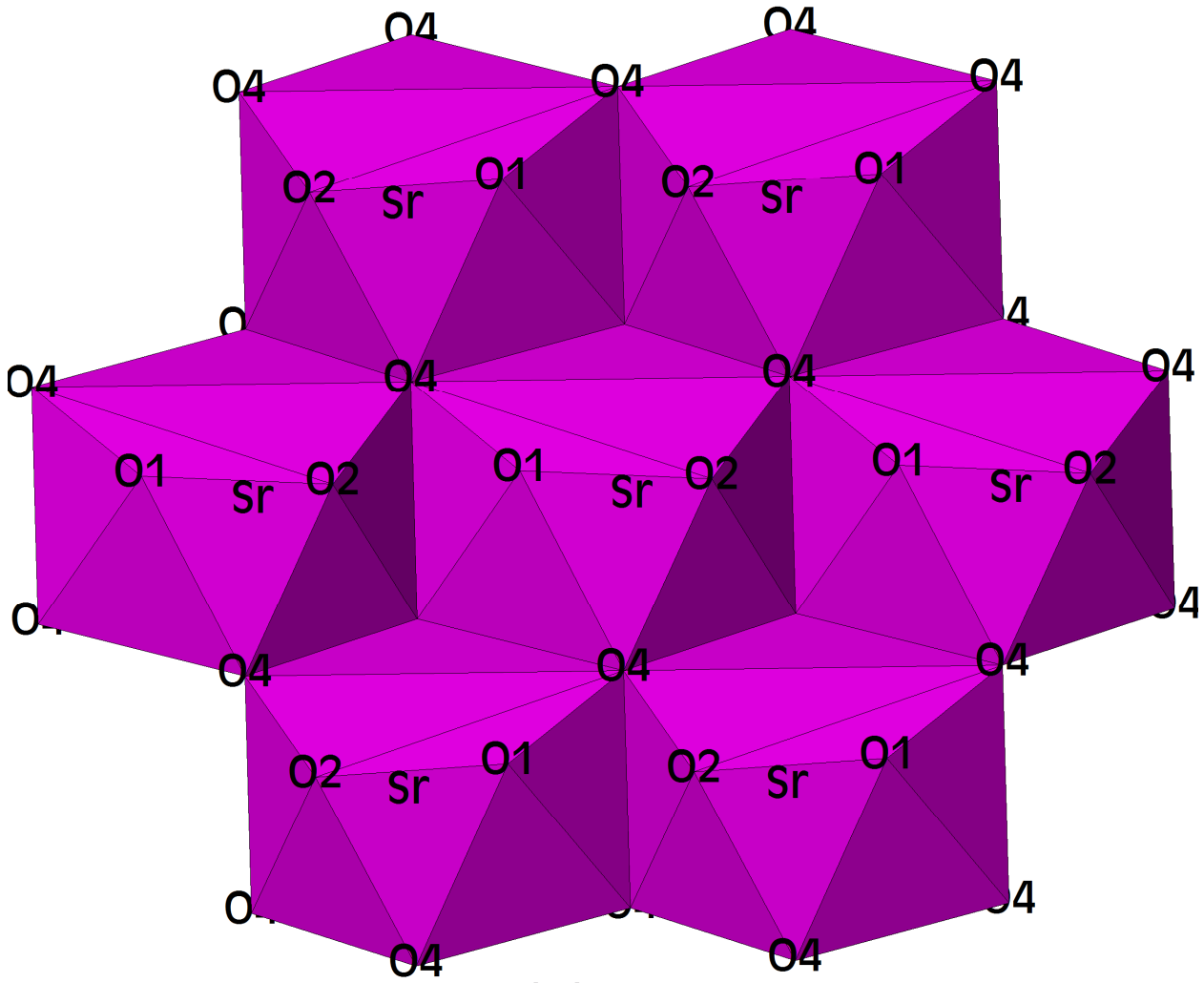
O4
O4
O4
O4
O2
Sr
O1
O2
Sr
O1
O4
O4
O4
O4
O1
Sr
O2
O1
Sr
O2
O1
Sr
O2
O4
O4
O4
O2
Sr
O1
O2
Sr
O1
O4
O4

(c)

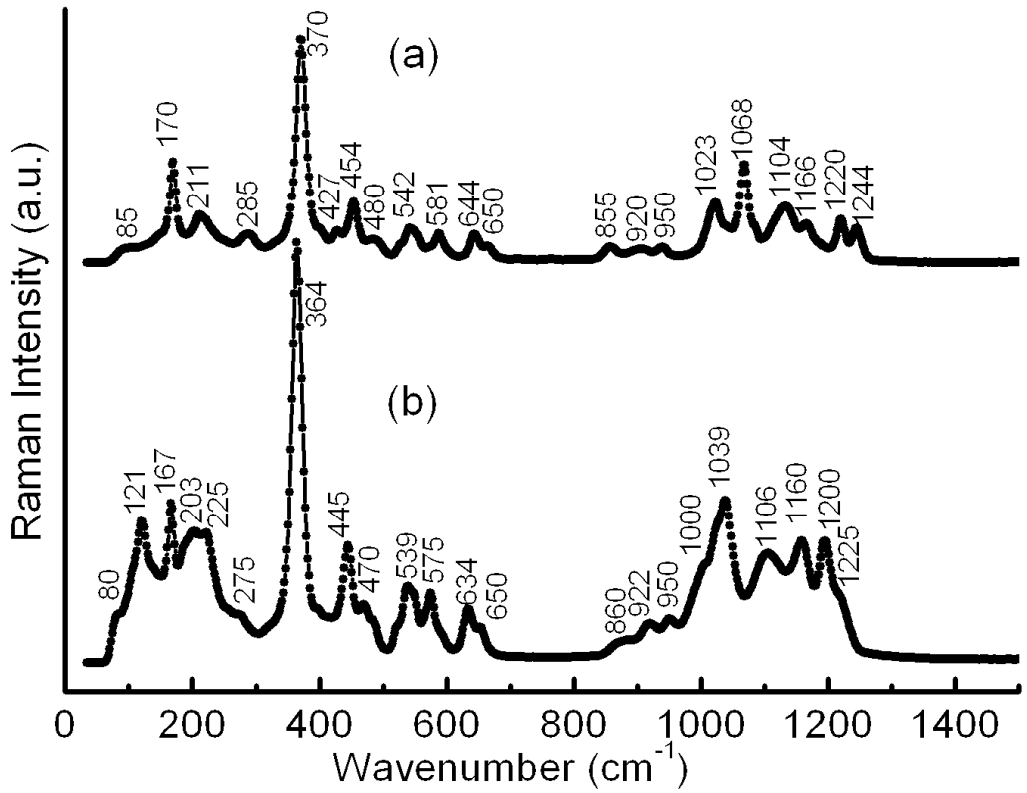
Raman Intensity (a.u.)
(a)
85
170
211
285
370
427
454
480
542
581
644
650
855
920
950
1023
1068
1104
1166
1220
1244
(b)
80
121
167
203
225
275
364
445
470
539
575
634
650
860
922
950
1000
1039
1106
1160
1200
1225
0
200
400
600
800
1000
1200
1400
Wavenumber (cm-1)

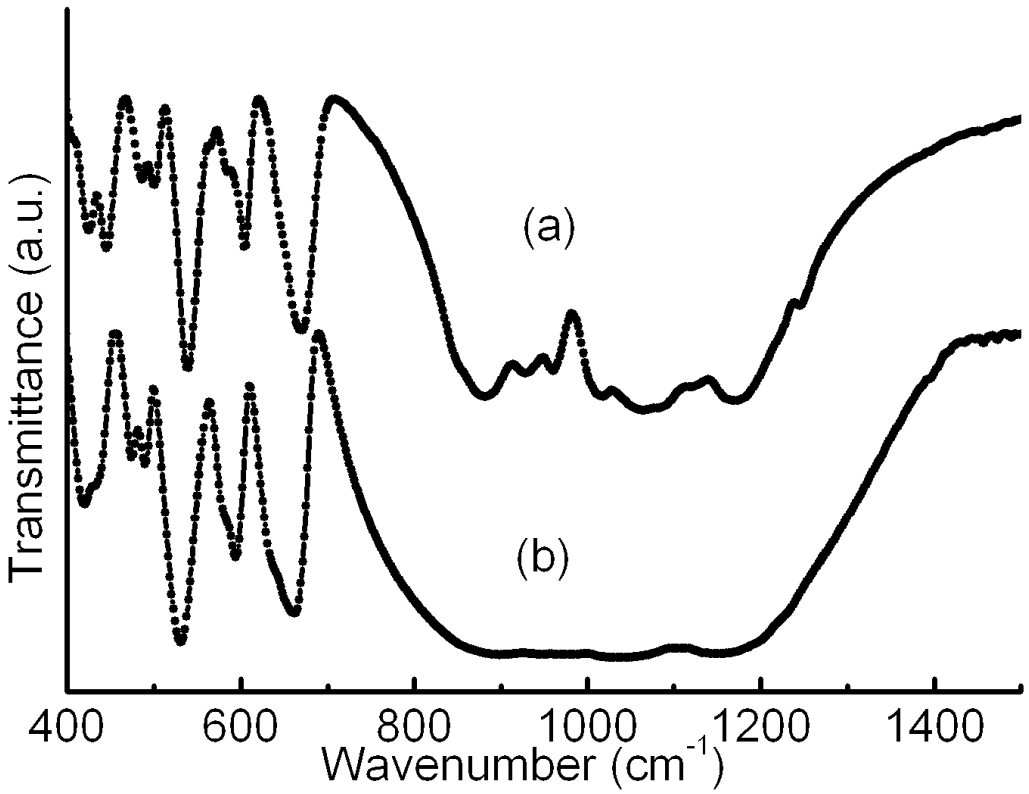

Highlights

-a new $A^{II}(Sb^{V}_{0.5}Fe^{III}_{0.5})(PO_4)_2$ (A = Sr, Pb, Ba) family of yavapaiite was described

-a strategy of structural determination was applied

- IR and Raman of $A^{II}Sb^{V}_{0.5}Fe^{III}_{0.5}(PO_4)_2$ (A = Sr, Pb) was studied